International Journal of Solids and Structures 51 (2014) 1758–1780

Contents lists available at ScienceDirect

International Journal of Solids and Structures

journal homepage: www.elsevier.com/locate/ijsolstr

Nonlocal elasticity defined by Eringen's integral model: Introduction of a boundary layer method

R. Abdollahi, B. Boroomand *

Department of Civil Engineering, Isfahan University of Technology, Isfahan 84156-83111, Iran

ARTICLE INFO

Article history:
Received 21 July 2013
Received in revised form 27 November 2013
Available online 28 January 2014

Keywords:
Nonlocal elasticity
Eringen's integral
Exponential basis functions
Trefftz method
Fundamental solutions
Boundary layer

ABSTRACT

In this paper we consider a nonlocal elasticity theory defined by Eringen's integral model and introduce, for the first time, a boundary layer method by presenting the exponential basis functions (EBFs) for such a class of problems. The EBFs, playing the role of the fundamental solutions, are found so that they satisfy the governing equations on an unbounded domain. Some insight to the theory is given by showing that the EBFs satisfying the Navier equations in the classical elasticity theory also satisfy the governing equations in the nonlocal theory. Some additional EBFs are particularly obtained for the nonlocal theory. In order to use the EBFs on bounded domains, the effects of the boundary conditions are taken into account by truncating the kernel/attenuation function in the constitutive equations. This leads to some residuals in the governing equations which appear near the boundaries. A weighted residual approach is employed to minimize the residuals near the boundaries. The method presented in this paper has much in common with Trefftz methods especially when the influence area of the kernel function is much smaller than the main computational domain. Several one/two dimensional problems are solved to demonstrate the way in which the EBFs can be used through the proposed boundary layer method.

© 2014 Elsevier Ltd. All rights reserved.

1. Introduction

Nonlocal elasticity models have received considerable attention by the researches intending to design or analyze Micro/Nano structures. The models extend the main concepts in the classical theory of elasticity to approximate the behavior of particles, as small as molecules or atoms, and therefore they play the role of models with bridging scales in the analysis of multi-scale problems. According to Eringen (1987), lack of an internal characteristic length in the classical theory limits the application of this theory in the modeling of physical problems in which the influence of microstructural effects is significant. The first attempts to modify the continuum approaches were made by Kröner (1967), Kunin (1984) and Krumhansl (1968). Improved formulations were proposed later by Edelen and Laws (1971), Edelen et al. (1971) and Eringen and Edelen (1972). Extensive studies by Eringen and Kim (1974) and Eringen et al. (1977) on nonlocal elasticity problems, with linear homogeneous and isotropic materials, must be mentioned here. The readers can find comprehensive surveys of nonlocal plasticity and damage models in the review papers by Bažant and Jirásek (2002) or Jirásek and Rolshoven (2003). More investigations on the choice of kernel function in nonlocal damage problems can be found in the studies by Borino et al. (2003).

Similar to the cases in the classical theories, the exact solution of problems defined with a nonlocal theory is almost impossible to achieve except for very few 1D cases. The readers may refer to the early studies by Pisano and Fuschi (2003), and more accurate and complete ones by Challamel and Wang (2008), Challamel et al. (2009a,b) and Benvenuti and Simone (2013). With the lack of analytical solutions, the use of numerical methods seems to be inevitable. The use of finite element method (FEM) has been reported in the studies by Polizzotto (2001) and Pisano et al. (2009). The studies by Schwartz et al. (2012) on the application of the boundary element method (BEM) should be mentioned here.

As indicated in almost all the aforementioned studies, the numerical solution of nonlocal elasticity problems is very time consuming. Therefore any mesh reduction approach may be considered vital in order to reduce the computational time. Nevertheless, as the numerical simulation tools are advancing, the lack of benchmark problems to access the capabilities of the numerical methods is increasingly felt especially in multi-dimensional cases. The objective of the recent studies by the authors is to attain such a goal (see Abdollahi and Boroomand, 2013). The paper presents a series of low-residual solutions for 1D and 2D problems using Chebyshev polynomials. Such polynomials proved to be useful in the solution of many problems in physics and engineering (see

* Corresponding author. Tel.: +98 311 3913817; fax: +98 311 3912700.
E-mail address: boromand@cc.iut.ac.ir (B. Boroomand).

http://dx.doi.org/10.1016/j.ijsolstr.2014.01.016
0020-7683/© 2014 Elsevier Ltd. All rights reserved.

Boyd, 2000) but of course may not play the role of fundamental solutions in nonlocal elasticity problems. Therefore, in order to solve the benchmark problems, some energy principles were used which require writing integral equations over the solution domain leading to a very expensive procedure (considering the integrals needed in the constitutive relations). Since the approach followed in that reference is extremely time consuming, the results of the benchmark solutions were given explicitly through a series of tables. The same approach may be followed for problems in 3D but of course the computational cost will be enormous.

In seeking low-residual solutions, one may think of using a Trefftz approach, as in the method of fundamental solutions (MFS) (see Kupradze and Aleksidze, 1964 or Fairweather and Karageorghis, 1998) or the BEM (see Brebbia and Dominguez, 1998) for instance, in which a series of predefined fundamental basis functions satisfying the governing equations are used (see also Zielinski and Herrera, 1987, Kita, 1995, Chen et al., 2009 for more details of Trefftz methods). However, the main hurdle in this way is the evaluation of the bases or the Green's functions. This paper deals with such a concept. After finding the fundamental bases, they may be used in a variety of simulation tools (letting alone the insight provided by them) including the one presented in this paper.

In this paper we first introduce some fundamental basis functions which fully satisfy the governing equations in a nonlocal elasticity theory defined by an integral constitutive low on unbounded domains. The bases are found in the form of exponential functions with complex exponents. The readers may find the application of similar bases to other engineering problems in the studies by Boroomand et al. (2010), Shamsaei and Boroomand (2011), Shahbazi et al. (2011a,b, 2012) and Azhari et al. (2013a,b) for static and time harmonic problems and the works by Zandi et al. (2012a,b), Hashemi et al. (2013), Movahedian et al. (2013) and Movahedian and Boroomand (2014) for transient problems (see also the extension of the method in Boroomand and Noormohammadi, 2013 for more general elasticity problems). In deriving such exponential basis functions (EBFs) we show that some of the bases are identical to those found for the classical elasticity theory earlier by the second author and co-workers (Boroomand et al., 2010). However, there are also some additional bases which are particularly found for the nonlocal theory. We present the closed form of the EBFs for 1D/2D problems using various attenuation/kernel functions. This gives an insight to the behavior of the material with nonlocal constitutive laws.

Having found the EBFs, we proceed to use them in a boundary layer approach. The term "boundary layer" stems from the fact that the use of the EBFs, defined on unbounded domains, in a bounded problem produces some residuals in a region close to the boundaries. To reduce such residuals, we employ a numerical approach with weights defined just on the boundary layer zone. With such features, the method may be classified in the Trefftz type of methods, similar to the BEM or MFS.

Letting alone the achievable accuracy by Trefftz methods, as is the case for the boundary layer method proposed here, the computational time saved by using them may be expected to be similar to the save of time when BEM and FEM codes are used. This especially becomes noticeable in the solution of problems defined on large domains with relatively small influence distance of nonlocal effect. The importance of this effect may be best understood when 3D problems are of concern. This, however, is beyond the scope of this paper.

In this paper, we demonstrate the capabilities of the method, in some 1D/2D problems, by comparing the results with the benchmark problems recently provided by the authors (Abdollahi and Boroomand, 2013) using Chebyshev polynomials.

The layout of the paper is as follows. In the next section we present an overview of the theory used in this paper. The way that the EBFs are extracted from the governing equation is explained in Section 3. In Section 4 we discuss on the choice of the attenuation/kernel function used. Section 5 is devoted to the introduction of a boundary layer method using the EBFs found. The numerical experiments are presented in Section 6 where we validate the results for 1D/2D problems. The conclusions made throughout the paper are summarized in Section 7.

2. Nonlocal model; an overview

We consider an elastic body occupying Ω in a 1D/2D space. The equilibrium equations in the local/nonlocal elasticity problems are written as

$$\mathbf{S}^T\boldsymbol{\sigma}+\mathbf{b}=\mathbf{0} \quad \text{in } \Omega. \tag{1}$$

The following boundary conditions are also considered

$$\mathbf{u}=\mathbf{u}_B \quad \text{on } \Gamma_u, \tag{2}$$

and

$$\tilde{\mathbf{n}}\boldsymbol{\sigma}=\mathbf{t} \quad \text{on } \Gamma_t. \tag{3}$$

In the above relations $\boldsymbol{\sigma}$ is the vector of stresses, $\mathbf{u}$ is the vector of displacements, $\mathbf{S}$ is the well-known operator for defining the strains as $\boldsymbol{\varepsilon}=\mathbf{Su}$, $\mathbf{b}$ is the vector of body force, $\mathbf{u}_B$ and $\mathbf{t}$ are the boundary displacement and tractions, respectively, and $\tilde{\mathbf{n}}$ is a matrix containing the components of the unit vector normal to the boundary for defining the tractions.

According to Eringen's model (2002) the stresses at a generic point as $\mathbf{x}=[x,y]^T$ are dependent on the strains at other points of the domain, here known as $\mathbf{x}'=[x',y']^T$. The strain and stress fields satisfy the following constitutive integral equation

$$\boldsymbol{\sigma}(\mathbf{x})=\int_\Omega k(\mathbf{x}',\mathbf{x})\,\mathbf{D}\,\boldsymbol{\varepsilon}(\mathbf{x}')\,\mathrm{d}\Omega_{\mathbf{x}'} \quad \forall \mathbf{x},\mathbf{x}'\in\Omega. \tag{4}$$

In the above relation $\mathbf{D}$ is the matrix of material constants as in the classical elasticity theory which is generally written as

$$\mathbf{D}=\begin{pmatrix} D_1 & D_2 & 0\\ D_2 & D_1 & 0\\ 0 & 0 & D_3\end{pmatrix} \tag{5}$$

for 2D problems. The attenuation/kernel function $k(\mathbf{x}',\mathbf{x})$ plays the role of a measure for the dependence of the stresses at $\mathbf{x}$ to the strains at $\mathbf{x}'$ (in (4) $\mathrm{d}\Omega_{\mathbf{x}'}$ denotes the volume fraction at $\mathbf{x}'$). When isotropy is of concern, which is the case in this study, $k(\mathbf{x}',\mathbf{x})$ is written as a function of the distance between $\mathbf{x}$ and $\mathbf{x}'$, i.e.

$$k(\mathbf{x}',\mathbf{x})=k(|\mathbf{x}'-\mathbf{x}|). \tag{6}$$

We use such a form in the rest of the formulation given in this paper. The function is chosen so that it reaches to its maximum at $\mathbf{x}=\mathbf{x}'$ and attenuates for large distances between $\mathbf{x}$ and $\mathbf{x}'$, i.e.

$$\lim_{|\mathbf{x}'-\mathbf{x}|\to\infty} k(|\mathbf{x}'-\mathbf{x}|)=0, \tag{7}$$

and also

$$\int_{\Omega_\infty} k(|\mathbf{x}'-\mathbf{x}|)\,\mathrm{d}\Omega=1, \tag{8}$$

analogous to a Dirac delta function, e.g. when a very sharp kernel function is used to recover the constitutive relations in the classical theory (in (8) Ω_∞ denotes an unbounded domain). It is clear that the sharpness of $k(|\mathbf{x}-\mathbf{x}'|)$ represents an internal characteristic length for the material.

An alternative nonlocal constitutive relation defined in Altan (1989) and Eringen (2002) incorporates the classical elasticity constitutive relation in a weighted fashion

$$\boldsymbol{\sigma}(\mathbf{x}) = \zeta_1 \mathbf{D}\,\boldsymbol{\varepsilon}(\mathbf{x}) + \zeta_2 \int_{\Omega} k(|\mathbf{x}' - \mathbf{x}|)\mathbf{D}\,\boldsymbol{\varepsilon}(\mathbf{x}')\,\mathrm{d}\Omega_{\mathbf{x}'}, \tag{9}$$

with ζ_1 and ζ_2 being two weight factors so that

$$\zeta_1 + \zeta_2 = 1. \tag{10}$$

Obviously by choosing $\zeta_1 = 0$ in (9) the constitutive equations convert to (4). The readers may also refer to the studies by Benvenuti and Tralli (2006), Challamel and Wang (2008) and Zingales et al. (2011) for a similar constitutive relation in nonlocal elasticity, and also those by Lazar et al. (2006) and Challamel (2013) for further assessment of a similar concept in nonlocal problems of bi-Helmholtz or beam type. Since the kernel function has a very small value at points far from the source point $\mathbf{x}$, it may be defined on a compact support within an influence distance L_R, i.e.

$$k(|\mathbf{x}' - \mathbf{x}|) = 0, \quad \forall |\mathbf{x}' - \mathbf{x}| > L_R. \tag{11}$$

The value of the influence distance L_R depends on the selected kernel function and the internal length (to be defined later). In Section 4 we shall give more details on the choice of the kernel function.

3. Exponential basis functions (EBFs)

In this section, residual-free EBFs are found for unbounded 1D/2D problems.

3.1. One-dimensional problems

The constitutive equation (9) for a bounded 1D problem is written as

$$\sigma(x) = \zeta_1 E\,\varepsilon(x) + \zeta_2 \int_0^L k(|x' - x|)E\,\varepsilon(x')\,\mathrm{d}x', \quad 0 \leqslant x \leqslant L, \tag{12}$$

in which E denotes the Young's modulus of the material. The boundary conditions are to be applied at $x = 0$ and $x = L$. To begin with, we neglect the boundary effects and consider an unbounded domain (or regions far from the boundaries) and rewrite the above equation as

$$\sigma(x) = \zeta_1 E\,\varepsilon(x) + \zeta_2 \int_{-\infty}^{\infty} k(|x' - x|)E\,\varepsilon(x')\,\mathrm{d}x'. \tag{13}$$

If $k(|x' - x|)$ is defined on a compact support as (11), then (13) is written as

$$\sigma(x) = \zeta_1 E\,\varepsilon(x) + \zeta_2 \int_{x-L_R}^{x+L_R} k(|x' - x|)E\,\varepsilon(x')\,\mathrm{d}x'. \tag{14}$$

Using a local coordinate as

$$\bar{x} = x' - x, \tag{15}$$

then Eq. (14) is rewritten as

$$\sigma(x) = \zeta_1 E\,\varepsilon(x) + \zeta_2 \int_{-L_R}^{L_R} k(|\bar{x}|)E\,\varepsilon(x + \bar{x})\,\mathrm{d}\bar{x}. \tag{16}$$

3.1.1. Homogenous part of the solution

Considering the homogeneous part of the solution, for the 1D problem, by substituting (16) in (1) the equilibrium equation takes the following form of

$$\frac{d}{dx}\left\{\zeta_1 E\,\varepsilon(x) + \zeta_2 \int_{-L_R}^{L_R} k(|\bar{x}|)E\,\varepsilon(x + \bar{x})\,\mathrm{d}\bar{x}\right\} = 0. \tag{17}$$

When the strain field is written in terms of the displacement field we have

$$\zeta_1 E \frac{d^2 u_H(x)}{dx^2} + \zeta_2 \frac{d}{dx}\left\{\int_{-L_R}^{L_R} k(|\bar{x}|)E\frac{du_H(x + \bar{x})}{dx}\,d\bar{x}\right\} = 0. \tag{18}$$

In (18), $u_H(x)$ denotes the homogeneous part of the solution. The EBFs may be evaluated by assuming

$$\hat{u}_H(x) = \sum_i c_i e^{\alpha_i x}. \tag{19}$$

Here $\hat{u}_H(x)$ plays the role of an approximation to the exact solution $u_H(x)$. By inserting (19) in (18) we arrive at

$$\sum_i c_i E \alpha_i^2 e^{\alpha_i x}\left(\zeta_1 + \zeta_2 \int_{-L_R}^{L_R} k(|\bar{x}|)\,e^{\alpha_i \bar{x}} d\bar{x}\right) = 0, \tag{20}$$

leading to the following characteristic equation

$$\alpha_i^2\left(\zeta_1 + \zeta_2 \int_{-L_R}^{L_R} k(|\bar{x}|)\,e^{\alpha_i \bar{x}} d\bar{x}\right) = 0. \tag{21}$$

The characteristic equation (21) must be solved for α_i. This leads to the following algebraic equations

$$\alpha_i^2 = 0, \quad \zeta_1 + \zeta_2 \int_{-L_R}^{L_R} k(|\bar{x}|)e^{\alpha_i \bar{x}} d\bar{x} = 0. \tag{22}$$

The first equation gives folded roots as $\alpha_i = 0$, which yields the well-known bases for the static analysis of a bar (i.e. 1 and x) in the classical theory of elasticity. The second equation in (22) must be solved numerically (more details will be given in Section 4). Depending on the choice of the kernel function $k(|\bar{x}|)$ different sets are obtained for α_i. The final solution is thus written as

$$\hat{u}_H(x) = c_1 + c_2 x + \sum_{i=2}^{N} c_i e^{\alpha_i x}, \tag{23}$$

where N is the number of all roots found (or to be used for the solution) for both equations in (22). Instead of working with the form given in the above relation, we prefer working with (19) as the compact form of (23).

Remark 1. The unknown coefficients in (19), or (23), are to be found from the information at the boundaries as well as the equilibrium conditions on the regions near boundaries when the EBFs are to be used on a bounded domain. It may be noted that at the points near boundaries falling in the support of the kernel function, the relations (13) or (14) are not valid. For instance when a generic point is considered near the end at $x = L$, the relation (14) should be replaced by

$$\sigma(x) = \zeta_1 E\,\varepsilon(x) + \zeta_2 \int_{-L_R}^{h} k(|\bar{x}|)E\,\varepsilon(x + \bar{x})\,\mathrm{d}\bar{x}, \tag{24}$$

with h being the distance between the point x, where the center of the kernel function is located, and the end point (i.e. $h = L - x$). Such a correction in the constitutive equation must be considered when the equilibrium equation (17) is written and thus the characteristic equation (21) does not represent the equilibrium condition. This shows that the EBFs found in (23) are suitable for a region $x \in [L_R, L - L_R]$ when the problem is to be solved on $[0, L]$. However, depending on the distance between the point x and either of the two ends, the deviation from full equilibrium state varies. This discussion indicates that when the nonlocal length is comparable with the dimension of the domain, i.e. $L/2 < L_R < L$, the series found in (23) will no longer satisfy the governing equation. However, the series may still be used for finding approximate solution in a fashion similar to our latest studies (Abdollahi and Boroomand, 2013).

Remark 2. The readers may note that when the kernel function is defined on an unbounded domain, as in (13), then the characteristic equation (21) takes the form of

$$\alpha_i^2\left(\zeta_1+\zeta_2\int_{-\infty}^{\infty}k(|\bar{x}|)\,e^{\alpha_i\bar{x}}d\bar{x}\right)=0. \tag{25}$$

In that case, regarding the discussion given in Remark 1, there will always be some residuals when the associated EBFs are used on a bounded domain. Nevertheless, when the generic point at x is far from the ends, the residuals are expected to be small due to the attenuation of the kernel function. Therefore finding the coefficients c_i just from the information at the boundaries and the equilibrium conditions near boundaries may seem to be appropriate. More details and discussions on such an effect will be presented in the section of numerical experiments.

3.1.2. Body forces in the 1D problems

When a body force is present in a 1D problem the solution to the problem may be performed by finding a particular part as u_P so that:

$$\zeta_1 E\frac{d^2u_P(x)}{dx^2}+\zeta_2\frac{d}{dx}\int_{-L_R}^{L_R}k(|\bar{x}|)E\frac{du_P(x+\bar{x})}{dx}d\bar{x}+b(x)=0, \tag{26}$$

where $b(x)$ is the body force. If $b(x)$ is expressed in terms of some exponential functions as

$$b(x)=\sum_r c_r e^{\alpha_r x}, \tag{27}$$

then the particular solution is also approximated as

$$\hat{u}_p(x)=\sum_r h_r e^{\alpha_r x}. \tag{28}$$

By substituting (27) and (28) in (26) one may evaluate the coefficients h_r as

$$h_r=\frac{-c_r}{E\alpha_r^2(\zeta_1+\zeta_2\int_{-L_R}^{L_R}k(|\bar{x}|)\,e^{\alpha_r\bar{x}}d\bar{x})}. \tag{29}$$

The displacement field is the sum of $\hat{u}_P$ and $\hat{u}_H$

$$\hat{u}(x)=\hat{u}_H+\hat{u}_p=\sum_i c_i e^{\alpha_i x}+\sum_r h_r e^{\alpha_r x}. \tag{30}$$

While α_i is determined from (22), α_r should be chosen so that the denominator in (29) does not vanish, i.e. α_r should not be chosen from the set found for α_i. The only unknowns in (30) are the coefficients c_i. The rest of the procedure, including the way that c_r is calculated and the set of α_r is chosen, is similar to the procedure described in Boroomand et al. (2010).

3.2. Two-dimensional problems

As in the 1D cases, we start from (9) while considering an unbounded domain Ω_∞

$$\boldsymbol{\sigma}(\mathbf{x})=\zeta_1\mathbf{D}\boldsymbol{\varepsilon}(\mathbf{x})+\zeta_2\int_{\Omega_\infty}k(|\mathbf{x}'-\mathbf{x}|)\mathbf{D}\boldsymbol{\varepsilon}(\mathbf{x}')\,d\Omega_{\mathbf{x}'}. \tag{31}$$

By defining a local coordinate system as

$$\bar{\mathbf{x}}=\mathbf{x}'-\mathbf{x}, \tag{32}$$

and using a kernel function $k(|\mathbf{x}'-\mathbf{x}|)$ defined on a compact support as (11), Eq. (31) is rewritten as

$$\boldsymbol{\sigma}(\mathbf{x})=\zeta_1\mathbf{D}\boldsymbol{\varepsilon}(\mathbf{x})+\zeta_2\int_{\Omega_s}k(|\bar{\mathbf{x}}|)\mathbf{D}\boldsymbol{\varepsilon}(\mathbf{x}+\bar{\mathbf{x}})\,d\Omega_s, \tag{33}$$

where Ω_s is the support of the kernel $k(|\mathbf{x}'-\mathbf{x}|)$.

3.2.1. Homogenous part of the solution

Considering the homogeneous part of the solution, by substituting (33) in (1) the equilibrium equations take the form of

$$\mathbf{S}^T\left\{\zeta_1\mathbf{D}\boldsymbol{\varepsilon}(\mathbf{x})+\zeta_2\int_{\Omega_s}k(|\bar{\mathbf{x}}|)\mathbf{D}\boldsymbol{\varepsilon}(\mathbf{x}+\bar{\mathbf{x}})\,d\Omega_s\right\}=\mathbf{0}. \tag{34}$$

When the strains are written in terms of the displacements we have

$$\mathbf{S}^T\left\{\zeta_1\mathbf{D}\mathbf{S}\mathbf{u}_H(\mathbf{x})+\zeta_2\int_{\Omega_s}k(|\bar{\mathbf{x}}|)\mathbf{D}\mathbf{S}\mathbf{u}_H(\mathbf{x}+\bar{\mathbf{x}})\,d\Omega_s\right\}=\mathbf{0}. \tag{35}$$

Here again $\mathbf{u}_H$ denotes the homogeneous part of the solution. The EBFs may be evaluated by assuming

$$\hat{\mathbf{u}}_H=\sum_i c_i\mathbf{h}^i_{(\alpha_i,\beta_i)}e^{\alpha_i x+\beta_i y}. \tag{36}$$

Here again $\hat{\mathbf{u}}_H$ is an approximation to $\mathbf{u}_H$. In (36) x and y are the coordinates of a generic point in Ω. The parameters α_i and β_i can take on complex values, that is $(\alpha_i,\beta_i)\in\mathbb{C}^2$. Also $\mathbf{h}^i_{(\alpha_i,\beta_i)}=[\,h_1^i\quad h_2^i\,]^T$ represents appropriate vectors to be found later. Substitution of (36) in (35) leads to the following relation

$$\sum_i c_i\begin{bmatrix}\alpha_i^2D_1+\beta_i^2D_3 & \alpha_i\beta_i(D_2+D_3)\\ \alpha_i\beta_i(D_2+D_3) & \alpha_i^2D_3+\beta_i^2D_1\end{bmatrix}\begin{Bmatrix}h_1^i\\ h_2^i\end{Bmatrix}g(\alpha_i,\beta_i)\,e^{\alpha_i x+\beta_i y}=\begin{Bmatrix}0\\0\end{Bmatrix}, \tag{37}$$

where $g(\alpha_i,\beta_i)$ is a function which is defined as

$$g(\alpha_i,\beta_i)=\left(\zeta_1+\zeta_2\int_{\Omega_s}k(|\bar{\mathbf{x}}|)e^{\alpha_i\bar{x}+\beta_i\bar{y}}d\Omega_s\right). \tag{38}$$

For the non-trivial solutions, the coefficients in the left hand side of (37), including the determinant of the coefficients matrix, must be set to zero. This leads to the following algebraic equations

$$(\alpha_i^2D_1+\beta_i^2D_3)(\alpha_i^2D_3+\beta_i^2D_1)-\alpha_i^2\beta_i^2(D_2+D_3)^2=0, \tag{39}$$

or

$$g(\alpha_i,\beta_i)=0. \tag{40}$$

From either of the above characteristic equations one may find α_i in terms of β_i or vice versa. An explicit relation will be given for $g(\alpha_i,\beta_i)$ in Section 4. When (40) is used, the characteristic vector $\mathbf{h}^i_{(\alpha_i,\beta_i)}$ takes an arbitrary form. However, when (39) is of concern, one should find an appropriate characteristic vector for the each pair of (α_i,β_i). To further elaborate on the EBFs, we consider a plane stress case in which

$$D_1=E/(1-\nu^2),\quad D_2=\nu D_1,\quad D_3=E/(2(1+\nu)), \tag{41}$$

where E and ν denote the Young's modulus and Poisson's ratio of the material, respectively. Substituting the material properties (41) in (39) and solving for α_i in terms of β_i we find

$$\alpha_i=\pm\mathbf{i}\beta_i\ \text{(folded roots)},\quad h_1^i=\pm\mathbf{i},\quad h_2^i=1,\quad \mathbf{i}=\sqrt{-1}, \tag{42}$$

or when β_i is calculated in terms of α_i

$$\beta_i=\pm\mathbf{i}\alpha_i\ \text{(folded roots)},\quad h_1^i=\mp\mathbf{i},\quad h_2^i=1. \tag{43}$$

It can be seen that the roots found are exactly the same as those in the classical elasticity theory reported in Boroomand et al. (2010). Moreover, similar to the classical elasticity theory, in each case some of the EBFs are missing. We follow the same procedure explained by Boroomand et al. (2010) in order to find the missing EBFs noting that in this case the equilibrium equations in (34) comprise additional terms. Therefore the missing EBFs are assumed to have the following general form

$$\hat{\mathbf{u}}_H^i = \left(\begin{Bmatrix} a_i^1 \\ a_i^2 \end{Bmatrix} x + \begin{Bmatrix} b_i^1 \\ b_i^2 \end{Bmatrix} y + \begin{Bmatrix} d_i^1 \\ d_i^2 \end{Bmatrix} \right) e^{\alpha_i x + \beta_i y}. \tag{44}$$

Introducing (44) in (35) leads to the following system of equations

$$\left\{ g(\alpha_i,\beta_i) \left(\mathbf{A} \begin{Bmatrix} a_i^1 \\ a_i^2 \end{Bmatrix} x + \mathbf{A} \begin{Bmatrix} b_i^1 \\ b_i^2 \end{Bmatrix} y \right) + g(\alpha_i,\beta_i) \left(\mathbf{A} \begin{Bmatrix} d_i^1 \\ d_i^2 \end{Bmatrix} + \mathbf{B} \begin{Bmatrix} a_i^1 \\ a_i^2 \end{Bmatrix} + \mathbf{C} \begin{Bmatrix} b_i^1 \\ b_i^2 \end{Bmatrix} \right) + \begin{Bmatrix} \alpha_i D_1 G_1 + \alpha_i D_2 G_2 + \beta_i D_3 G_3 \\ \beta_i D_2 G_1 + \beta_i D_1 G_2 + \alpha_i D_3 G_3 \end{Bmatrix} \right\} e^{\alpha_i x + \beta_i y} = \begin{Bmatrix} 0 \\ 0 \end{Bmatrix}, \tag{45}$$

with $\mathbf{A}$ being the same coefficient matrix as in (37) and

$$\mathbf{B} = \begin{bmatrix} 2D_1\alpha_i & (D_2+D_3)\beta_i \\ (D_2+D_3)\beta_i & 2D_3\alpha_i \end{bmatrix}, \quad \mathbf{C} = \begin{bmatrix} 2D_3\beta_i & (D_2+D_3)\alpha_i \\ (D_2+D_3)\alpha_i & 2D_1\beta_i \end{bmatrix}. \tag{46}$$

Also G_1, G_2 and G_3 in (45) are evaluated by the following expressions

$$\begin{Bmatrix} G_1 \\ G_2 \\ G_3 \end{Bmatrix} = \zeta_2 \int_{\Omega_s} k(|\bar{\mathbf{x}}|) e^{\alpha_i \bar{x} + \beta_i \bar{y}} \begin{Bmatrix} \alpha_i (a_i^1 \bar{x} + b_i^1 \bar{y}) \\ \beta_i (a_i^2 \bar{x} + b_i^2 \bar{y}) \\ \alpha_i (a_i^2 \bar{x} + b_i^2 \bar{y}) + \beta_i (a_i^1 \bar{x} + b_i^1 \bar{y}) \end{Bmatrix} d\Omega_s. \tag{47}$$

Since the determinant of $\mathbf{A}$ vanishes, one may choose

$$\alpha_i = \pm \mathbf{i} \beta_i \rightarrow \begin{Bmatrix} a_i^1 \\ a_i^2 \end{Bmatrix} = a \begin{Bmatrix} \pm \mathbf{i} \\ 1 \end{Bmatrix}, \quad \begin{Bmatrix} b_i^1 \\ b_i^2 \end{Bmatrix} = b \begin{Bmatrix} \pm \mathbf{i} \\ 1 \end{Bmatrix} \tag{48}$$

or

$$\beta_i = \pm \mathbf{i} \alpha_i \rightarrow \begin{Bmatrix} a_i^1 \\ a_i^2 \end{Bmatrix} = a \begin{Bmatrix} \mp \mathbf{i} \\ 1 \end{Bmatrix}, \quad \begin{Bmatrix} b_i^1 \\ b_i^2 \end{Bmatrix} = b \begin{Bmatrix} \mp \mathbf{i} \\ 1 \end{Bmatrix}. \tag{49}$$

By using the above values, the last term in (45) vanishes and now by setting to zero the second term in (45) the following sets for $\mathbf{u}_H^i$ are obtained

$$\alpha_i = \pm \mathbf{i} \beta_i \rightarrow \mathbf{u}_H^i = \left(a \begin{Bmatrix} \pm \mathbf{i} \\ 1 \end{Bmatrix} x + b \begin{Bmatrix} \pm \mathbf{i} \\ 1 \end{Bmatrix} y + \begin{Bmatrix} p(a,b) \\ d(a,b) \end{Bmatrix} \right) e^{\alpha_i x + \beta_i y}, \tag{50}$$

or

$$\beta_i = \pm \mathbf{i} \alpha_i \rightarrow \mathbf{u}_H^i = \left(a \begin{Bmatrix} \mp \mathbf{i} \\ 1 \end{Bmatrix} x + b \begin{Bmatrix} \mp \mathbf{i} \\ 1 \end{Bmatrix} y + \begin{Bmatrix} q(a,b) \\ d(a,b) \end{Bmatrix} \right) e^{\alpha_i x + \beta_i y}, \tag{51}$$

where a, b are two arbitrary coefficients while p, q and d are three functions of a, b. This leads to four additional bases, one for each root. Our experience in the classical elasticity problems shows that combining the bases given in (50) or (51) still produces excellent results while decreasing the number of bases from six to four (see Boroomand et al., 2010; Shamsaei and Boroomand, 2011, and Zandi et al., 2012b). We use ($a = b = 1$) which leads to $d = 1$ and

$$p = \frac{\pm \mathbf{i}(\beta_i + (1 - \mathbf{i})(3 - 4\nu))}{\beta_i} \quad \text{or} \quad q = \frac{\mathbf{i}(\alpha_i + (1 \pm \mathbf{i})(3 - 4\nu))}{\alpha_i}. \tag{52}$$

The final set of the EBFs may be written as (for $\alpha_i = \pm \mathbf{i} \beta_i$)

$$\begin{aligned} \hat{\mathbf{u}}_H = \sum_i \Bigg\{ & c_i^1 \begin{bmatrix} \mathbf{i} \\ 1 \end{bmatrix} e^{\beta_i(\mathbf{i}x+y)} + c_i^2 \begin{bmatrix} -\mathbf{i} \\ 1 \end{bmatrix} e^{\beta_i(-\mathbf{i}x+y)} \\ & + c_i^3 \left(\begin{bmatrix} \mathbf{i} \\ 1 \end{bmatrix} x + \begin{bmatrix} \mathbf{i} \\ 1 \end{bmatrix} y + \begin{bmatrix} \frac{\mathbf{i}\beta_i(1+\nu)+(1-\mathbf{i})(\nu-3)}{\beta_i(1+\nu)} \\ 1 \end{bmatrix} \right) e^{\beta_i(\mathbf{i}x+y)} \\ & + c_i^4 \left(\begin{bmatrix} -\mathbf{i} \\ 1 \end{bmatrix} x + \begin{bmatrix} -\mathbf{i} \\ 1 \end{bmatrix} y + \begin{bmatrix} \frac{-\mathbf{i}\beta_i(1+\nu)+(1+\mathbf{i})(\nu-3)}{\beta_i(1+\nu)} \\ 1 \end{bmatrix} \right) e^{\beta_i(-\mathbf{i}x+y)} \Bigg\} \\ & + \sum_j \bar{c}_j^1 \begin{bmatrix} 1 \\ 0 \end{bmatrix} e^{\alpha_j x + \beta_j y} + \sum_j \bar{c}_j^2 \begin{bmatrix} 0 \\ 1 \end{bmatrix} e^{\alpha_j x + \beta_j y}. \end{aligned} \tag{53}$$

The EBFs for the case of $\beta_i = \pm \mathbf{i} \alpha_i$ may be obtained analogously (also for plane strain cases). As is seen, the first four forms in (53) are identical to those obtained by Boroomand et al. (2010) for the classical elasticity problems. The last two forms in (53) pertain to the characteristic equation (40). It may suffice to mention that we choose α and β based on the strategy suggested in our previous study (Boroomand et al., 2010).

Obviously the EBFs found as in (53) are suitable when the kernel support does not intersect the boundaries of the domain (see Remark 1).

3.2.2. Body forces in the 2D problems

Similar to the 1D problems, the particular part of the solution in 2D cases is written as:

$$\hat{\mathbf{u}}_P = \sum_{r,s} \mathbf{h}_{rs} e^{\alpha_r x + \beta_s y}, \tag{54}$$

where α_r and β_s are two independent complex numbers to be chosen so that $g(\alpha_r, \beta_s) \neq 0$ and also the determinant of the coefficient matrix in (37) does not vanish. Also $\mathbf{h}_{rs}$ represents a set of vectors containing the coefficients that are to be evaluated by substituting (54) in (1) while expressing the body forces $\mathbf{b}$ in terms of EBFs. The procedure of finding $\mathbf{h}_{rs}$ is similar to that explained in Boroomand et al. (2010) and thus we do not repeat it here for the sake of conciseness. The approximated displacement field is the sum of $\hat{\mathbf{u}}_p$ in (54) and $\hat{\mathbf{u}}_H$ in (53)

$$\hat{\mathbf{u}} = \hat{\mathbf{u}}_p + \hat{\mathbf{u}}_H. \tag{55}$$

The unknown coefficients in (53) are determined by the use of a weighted residual approach (see Section 5).

4. The choice of the kernel function

In this section we present more details on the choice of the kernel function k and the associated characteristic equations in the 1D/2D problems.

4.1. One-dimensional problems

For 1D problems the following kernel function is used (see for instance Pisano and Fuschi, 2003)

$$k(|\bar{x}|) = \frac{1}{2l} e^{-\frac{|\bar{x}|}{l}}. \tag{56}$$

In the above relation l is a characteristic length depending on the material micro-mechanical properties. Note that k in (56) has been normalized so that (8) holds. In this paper we also use the following kernel

$$k(|\bar{x}|) = \frac{1}{l\sqrt{\pi}} e^{-\frac{\bar{x}^2}{l^2}}, \tag{57}$$

which is consistent with the kernel used for the 2D problems (see Section 4.2).

When (56) is used as the kernel, the characteristic equation in (22) does not have closed form solution and thus it must be solved numerically. Finding the roots of such a characteristics equation is a tedious task. We present a number of its roots for various values of L_R/l in Appendix B. If the kernel in (56) is defined on an unbounded domain, i.e. $L_R \to \infty$, then the characteristic equation takes the following form

$$\zeta_1 + \frac{\zeta_2}{1 - l^2\alpha_i^2} = 0. \tag{58}$$

The above equation possesses just two roots as $\alpha_i = \pm\sqrt{\zeta_1 + \zeta_2}/l\sqrt{\zeta_1}$. Such a set of roots is not sufficient for constructing a series of EBFs (instead one may use the roots presented in Appendix B when L_R/l is relatively large).

Alternatively, when (57) is used as the kernel the following characteristic equation is obtained

$$\zeta_1 + \frac{1}{2}e^{\frac{1}{4}l^2\alpha_i^2}\zeta_2\left[Erf\left(\frac{L_R}{l} - \frac{l\alpha_i}{2}\right) + Erf\left(\frac{L_R}{l} + \frac{l\alpha_i}{2}\right)\right] = 0. \tag{59}$$

In the above relation $Erf(.)$ denotes the error function, i.e.

$$Erf(x) = \frac{2}{\sqrt{\pi}}\int_0^x e^{-s^2}ds. \tag{60}$$

It can be seen that still finding the roots of such equation is a tedious task. However, when the kernel (57) is defined on an unbounded support/domain ($L_R \to \infty$) we obtain the following equation whose roots are found easily

$$\zeta_1 + \zeta_2 e^{\frac{l^2\alpha_i^2}{4}} = 0. \tag{61}$$

To find an explicit relation for the roots of (61) we rewrite it as

$$\frac{\zeta_2}{\zeta_1}e^{\frac{l^2\alpha_i^2}{4}} = -1 = e^{(2n-1)\mathbf{i}\pi}, \quad n \in \mathbb{Z}. \tag{62}$$

This leads to the following relation for the roots

$$\alpha_i = \pm\frac{2\sqrt{(2n-1)\mathbf{i}\pi + \ln(\zeta_1/\zeta_2)}}{l}, \quad \zeta_1 \neq 0,\ \zeta_2 \neq 0. \tag{63}$$

Nevertheless, the relation in (63) is not valid for $\zeta_1 = 0$, i.e. pure nonlocal elasticity case (note that $\zeta_2 = 0$ refers to the classical theory). For $\zeta_1 = 0$ one may directly use (59) for a finite value of L_R (see Appendix C for this case). The variation of the first two EBFs constructed by the roots obtained in (63), the roots of (59) and those given in Appendix B for the first kernel (56) is shown in Fig. 1. For simplicity we have considered a normalized coordinate as $\xi = x/L$ and a bounded domain as $0 \leqslant \xi \leqslant 1$ for plotting the EBFs (although they are defined for $\xi \in (-\infty, \infty)$). The EBFs are normalized with respect to their maximum which happens at either of the end points. As is seen in Fig. 1(a) both sets of EBFs constructed by the roots given as (63) and those obtained for (59) are similar. Fig. 1(b) depicts that the EBFs constructed by the roots of the characteristic equation using the first kernel are different from those in Fig. 1(a). All EBFs attenuate fast from both ends towards the mid points of the interval $0 \leqslant \xi \leqslant 1$. This indicates that for a bounded domain with no body force, the nonlocal effect may be expected at regions near the boundaries. This means that the bases obtained for the classical elasticity theory, as the first two in (23) for the 1D cases, are good choices (or perhaps enough) for the solution at the middle part of the problem.

4.2. Two-dimensional problems

For 2D problems the following kernel function is used (see for instance Polizzotto, 2001 and Pisano et al., 2009)

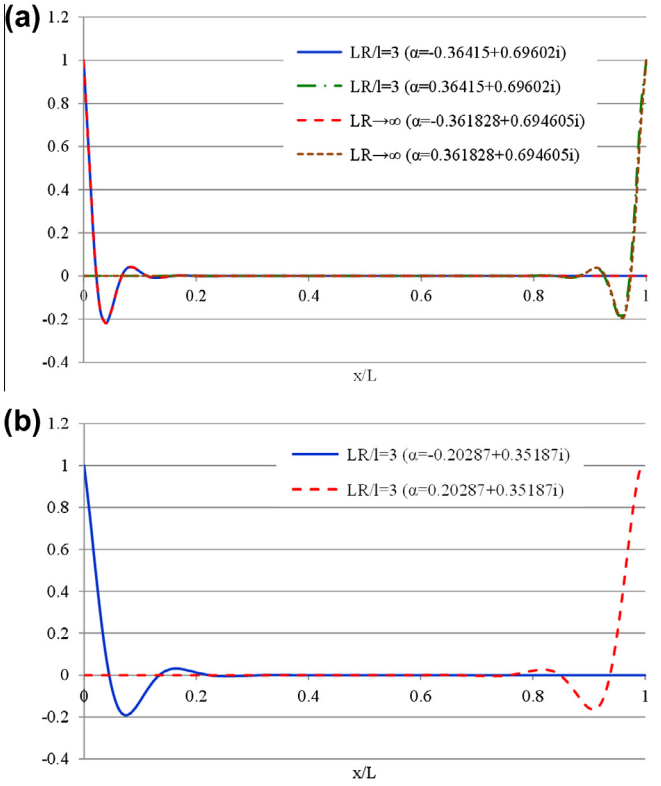

Fig. 1. Variation of the EBFs found for the 1D cases and for $l = L/20$; and $\zeta_1/\zeta_2 = 1/9$; (a) from the roots of the Eq. in (59) for finite L_R and those evaluated as in (63) for $L_R \to \infty$ for the kernel in (57), (b) from the roots of the characteristic equation obtained for the kernel in (56).

$$k(|\bar{\mathbf{x}}|) = \frac{1}{\pi l^2}e^{-\frac{\bar{x}^2+\bar{y}^2}{l^2}}. \tag{64}$$

The characteristic equation in (40) takes the following form

$$g(\alpha_i, \beta_i) = \zeta_1 + \frac{1}{4}e^{\frac{1}{4}l^2(\alpha_i^2+\beta_i^2)}\zeta_2\left[Erf\left(\frac{L_R}{l} - \frac{l\alpha_i}{2}\right) + Erf\left(\frac{L_R}{l} + \frac{l\alpha_i}{2}\right)\right]\left[Erf\left(\frac{L_R}{l} - \frac{l\beta_i}{2}\right) + Erf\left(\frac{L_R}{l} + \frac{l\beta_i}{2}\right)\right] = 0. \tag{65}$$

Similar to (59) finding the roots of $g(\alpha_i, \beta_i)$ is not an easy task. Instead one may think of using the kernel on an unbounded domain which leads to the following characteristic equation

$$g(\alpha_i, \beta_i) = \zeta_1 + \zeta_2 e^{\frac{l^2}{4}(\alpha_i^2+\beta_i^2)} = 0. \tag{66}$$

Following a similar procedure for deriving explicit relations for the roots of (61), we may write

$$\alpha_i^2 + \beta_i^2 = \frac{4(2n-1)\mathbf{i}\pi + 4\ln(\zeta_1/\zeta_2)}{l^2}, \quad n \in \mathbb{Z},\ \zeta_1 \neq 0,\ \zeta_2 \neq 0. \tag{67}$$

From which α_i may be evaluated in terms of β_i or vice versa. To give more insight to the behavior of the EBFs, their variation is shown in Fig. 2 for a set of pairs of (α, β). Here again, although the functions are defined on an unbounded domain, they are plotted on a bounded domain $0 \leqslant \xi \leqslant 1$, $0 \leqslant \eta \leqslant 1$ with $\xi = x/a$ and $\eta = y/b$ for a rectangular domain $a \times b$. The EBFs are normalized with respect to their maximum values in the region. Similar to the 1D cases, it can be seen that the functions attenuate fast towards the interior parts of the bounded domain. This means that

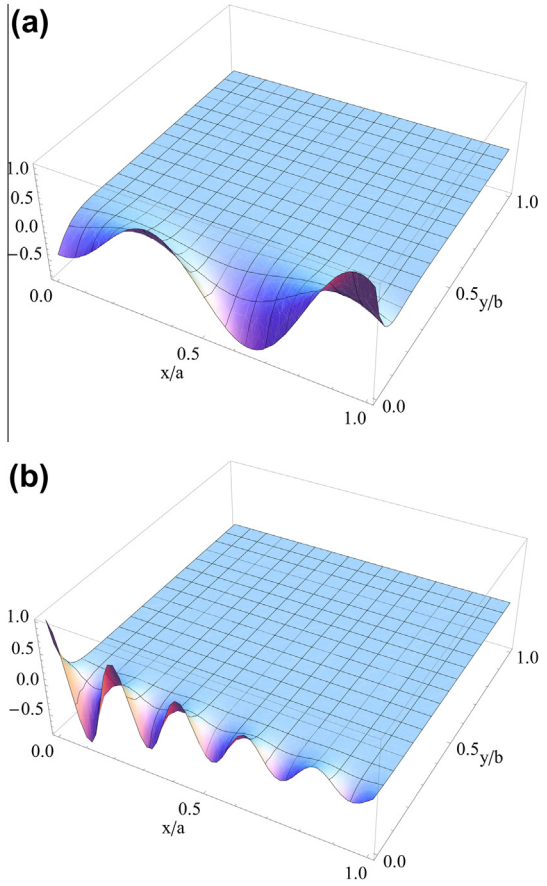

Fig. 2. Variation of the EBFs found for the 2D cases from Eq. (67) and for $l = a/5$ (*or* $b/5$) and $\zeta_1/\zeta_2 = 1$ and $n = 1$; (a) for $\alpha = 0.01 - 0.1i$, $\beta = -0.1496 - 0.1117i$, (b) for $\alpha = -0.02 - 0.3i$, $\beta = -0.3011 - 0.0322i$.

the basis functions found for the classical elasticity theory as in (53) play a key role in the solution at the interior parts of a bounded domain.

The readers may note again that the relation in (67) is not valid for $\zeta_1 = 0$. Nevertheless, for such a case one may still use (65) for a finite value of L_R. Interesting to note is that for $\zeta_1 = 0$ two independent sets are obtained for α_i and β_i each of which is similar to the set of roots evaluated for the relation in the 1D cases in (59) when $\zeta_1 = 0$. This means that the roots reported in Appendix C for the relation in (59) may be used for the 2D cases.

5. A boundary layer method using a weighted residual approach

In this section we use the EBFs found earlier to develop a boundary layer method. The term "boundary layer' is used to indicate that the method uses the boundary information, similar to other methods such as the BEM, as well as the information at a layer/region close to the boundary (see Remark 1). However, as indicated in Remark 2, by using the EBFs suitable for unbounded domains there always will be some residuals when they are used for the solution of problems on bounded domains. However the effect becomes immaterial at the interior parts when the length of nonlocal effect is sufficiently small in comparison with the size of the main computational domain (see Section 4). We shall present the details of such an effect in the section of numerical experiments.

5.1. One-dimensional problems

In the 1D problems defined on $[0, L]$ we write a weighted residual expression

$$\int_0^L w_l(x)\left[\frac{d}{dx}\left\{\zeta_1 E\hat{\varepsilon}(x)+\zeta_2\int_{-L_R}^{L_R}k(|\bar{x}|)E\hat{\varepsilon}(x+\bar{x})\,d\bar{x}\right\}+b(x)\right]dx=0, \tag{68}$$

where $w_l(x)$ represents a set of weight functions and $\hat{\varepsilon}$ is the approximated strain field to be evaluated from $\hat{u}$. Note that in the above relation we have considered the body forces and thus when the strain field is written in terms of the displacement field, in view of (30), we should write

$$\int_0^L w_l(x)\left[\frac{d}{dx}\left\{\zeta_1 E\frac{d(\hat{u}_H(x)+\hat{u}_P(x))}{dx} +\zeta_2\int_{-L_R}^{L_R}k(|\bar{x}|)E\frac{d(\hat{u}_H(x+\bar{x})+\hat{u}_P(x+\bar{x}))}{dx}\,d\bar{x}\right\}+b(x)\right]dx=0, \tag{69}$$

which may be rearranged as

$$\int_0^L w_l(x)\left[\frac{d}{dx}\left\{\zeta_1 E\frac{d\hat{u}_H(x)}{dx}+\zeta_2\int_{-L_R}^{L_R}k(|\bar{x}|)E\frac{d\hat{u}_H(x+\bar{x})}{dx}\,d\bar{x}\right\}\right]dx + \int_0^L w_l(x)\left[\frac{d}{dx}\left\{\zeta_1 E\frac{d\hat{u}_P(x)}{dx}+\zeta_2\int_{-L_R}^{L_R}k(|\bar{x}|)E\frac{d\hat{u}_P(x+\bar{x})}{dx}\,d\bar{x}\right\} +b(x)\right]dx=0. \tag{70}$$

One can use a set of piece-wise continuous functions for $w_l(x)$, similar to the hat-functions in the finite element method. The definition of $w_l(x)$ may be given as

$$\begin{cases} w_l(x)=0 & x\leqslant x_l-L_w/2,\\ w_l(x)\neq 0 & x_l-L_w/2\leqslant x\leqslant x_l+L_w/2\,,\\ w_l(x)=0 & x_l+L_w/2\leqslant x. \end{cases} \tag{71}$$

In such a case the relation in (70) may be written on seven parts of the domain (assuming that L_R is discretized by a number of cells with equal sizes while $L_R \ll L$) as

$$\int_0^{L_w/2} w_l(x)\left[\frac{d}{dx}\left\{\zeta_1 E\frac{d\hat{u}_H(x)}{dx}+\zeta_2\int_{-x}^{L_R}k(|\bar{x}|)E\frac{d\hat{u}_H(x+\bar{x})}{dx}\,d\bar{x}\right\}\right]dx + \int_0^{L_w/2} w_l(x)\left[\frac{d}{dx}\left\{\zeta_1 E\frac{d\hat{u}_P(x)}{dx}+\zeta_2\int_{-x}^{L_R}k(|\bar{x}|)E\frac{d\hat{u}_P(x+\bar{x})}{dx}\,d\bar{x}\right\}+b(x)\right]dx =0,\quad x_l=0, \tag{72}$$

and

$$\int_{x_l-\frac{L_w}{2}}^{x_l+\frac{L_w}{2}} w_l(x)\left[\frac{d}{dx}\left\{\zeta_1 E\frac{d\hat{u}_H(x)}{dx}+\zeta_2\int_{-x}^{L_R}k(|\bar{x}|)E\frac{d\hat{u}_H(x+\bar{x})}{dx}\,d\bar{x}\right\}\right]dx + \int_{x_l-\frac{L_w}{2}}^{x_l+\frac{L_w}{2}} w_l(x)\left[\frac{d}{dx}\left\{\zeta_1 E\frac{d\hat{u}_P(x)}{dx}+\zeta_2\int_{-x}^{L_R}k(|\bar{x}|)E\frac{d\hat{u}_P(x+\bar{x})}{dx}\,d\bar{x}\right\}+b(x)\right]dx=0,$$

$$\frac{L_w}{2}\leqslant x_l\leqslant L_R-\frac{L_w}{2},$$

and

$$\int_{x_I-\frac{L_w}{2}}^{L_R} w_I(x)\left[\frac{d}{dx}\left\{\zeta_1 E\frac{d\hat{u}_H(x)}{dx}+\zeta_2\int_{-x}^{L_R}k(|\bar{x}|)E\frac{d\hat{u}_H(x+\bar{x})}{dx}\,d\bar{x}\right\}\right]dx$$
$$+\int_{L_R}^{x_I+\frac{L_w}{2}} w_I(x)\left[\frac{d}{dx}\left\{\zeta_1 E\frac{d\hat{u}_H(x)}{dx}\right.\right.$$
$$\left.\left.+\zeta_2\int_{-L_R}^{L_R}k(|\bar{x}|)E\frac{d\hat{u}_H(x+\bar{x})}{dx}\,d\bar{x}\right\}\right]dx$$
$$+\int_{x_I-\frac{L_w}{2}}^{L_R} w_I(x)\left[\frac{d}{dx}\left\{\zeta_1 E\frac{d\hat{u}_P(x)}{dx}\right.\right.$$
$$\left.\left.+\zeta_2\int_{-x}^{L_R}k(|\bar{x}|)E\frac{d\hat{u}_P(x+\bar{x})}{dx}\,d\bar{x}\right\}+b(x)\right]dx$$
$$+\int_{L_R}^{x_I+\frac{L_w}{2}} w_I(x)\left[\frac{d}{dx}\left\{\zeta_1 E\frac{d\hat{u}_P(x)}{dx}\right.\right.$$
$$\left.\left.+\zeta_2\int_{-L_R}^{L_R}k(|\bar{x}|)E\frac{d\hat{u}_P(x+\bar{x})}{dx}\,d\bar{x}\right\}+b(x)\right]dx=0,$$
$$L_R-\frac{L_w}{2}<x_I<L_R+\frac{L_w}{2}, \tag{74}$$

and

$$\int_{x_I-\frac{L_w}{2}}^{x_I+\frac{L_w}{2}} w_I(x)\left[\frac{d}{dx}\left\{\zeta_1 E\frac{d\hat{u}_H(x)}{dx}+\zeta_2\int_{-L_R}^{L_R}k(|\bar{x}|)E\frac{d\hat{u}_H(x+\bar{x})}{dx}\,d\bar{x}\right\}\right]dx$$
$$+\int_{x_I-\frac{L_w}{2}}^{x_I+\frac{L_w}{2}} w_I(x)\left[\frac{d}{dx}\left\{\zeta_1 E\frac{d\hat{u}_P(x)}{dx}\right.\right.$$
$$\left.\left.+\zeta_2\int_{-L_R}^{L_R}k(|\bar{x}|)E\frac{d\hat{u}_P(x+\bar{x})}{dx}\,d\bar{x}\right\}+b(x)\right]dx=0,$$
$$L_R+\frac{L_w}{2}\leqslant x_I\leqslant L-L_R-\frac{L_w}{2}, \tag{75}$$

$$\int_{x_I-\frac{L_w}{2}}^{L-L_R} w_I(x)\left[\frac{d}{dx}\left\{\zeta_1 E\frac{d\hat{u}_H(x)}{dx}+\zeta_2\int_{-L_R}^{L_R}k(|\bar{x}|)E\frac{d\hat{u}_H(x+\bar{x})}{dx}\,d\bar{x}\right\}\right]dx$$
$$+\int_{L-L_R}^{x_I+\frac{L_w}{2}} w_I(x)\left[\frac{d}{dx}\left\{\zeta_1 E\frac{d\hat{u}_H(x)}{dx}\right.\right.$$
$$\left.\left.+\zeta_2\int_{-L_R}^{L-x}k(|\bar{x}|)E\frac{d\hat{u}_H(x+\bar{x})}{dx}\,d\bar{x}\right\}\right]dx$$
$$+\int_{x_I-\frac{L_w}{2}}^{L-L_R} w_I(x)\left[\frac{d}{dx}\left\{\zeta_1 E\frac{d\hat{u}_P(x)}{dx}\right.\right.$$
$$\left.\left.+\zeta_2\int_{-L_R}^{L_R}k(|\bar{x}|)E\frac{d\hat{u}_P(x+\bar{x})}{dx}\,d\bar{x}\right\}+b(x)\right]dx$$
$$+\int_{L-L_R}^{x_I+\frac{L_w}{2}} w_I(x)\left[\frac{d}{dx}\left\{\zeta_1 E\frac{d\hat{u}_P(x)}{dx}\right.\right.$$
$$\left.\left.+\zeta_2\int_{-L_R}^{L-x}k(|\bar{x}|)E\frac{d\hat{u}_P(x+\bar{x})}{dx}\,d\bar{x}\right\}+b(x)\right]dx=0,$$
$$L-L_R-\frac{L_w}{2}<x_I<L-L_R+\frac{L_w}{2}, \tag{76}$$

and

$$\int_{x_I-\frac{L_w}{2}}^{x_I+\frac{L_w}{2}} w_I(x)\left[\frac{d}{dx}\left\{\zeta_1 E\frac{d\hat{u}_H(x)}{dx}+\zeta_2\int_{-L_R}^{L-x}k(|\bar{x}|)E\frac{d\hat{u}_H(x+\bar{x})}{dx}\,d\bar{x}\right\}\right]dx$$
$$+\int_{x_I-\frac{L_w}{2}}^{x_I+\frac{L_w}{2}} w_I(x)\left[\frac{d}{dx}\left\{\zeta_1 E\frac{d\hat{u}_P(x)}{dx}+\zeta_2\int_{-L_R}^{L-x}k(|\bar{x}|)E\frac{d\hat{u}_P(x+\bar{x})}{dx}\,d\bar{x}\right\}+b(x)\right]dx$$
$$=0,\ L-L_R+\frac{L_w}{2}\leqslant x_I\leqslant L-\frac{L_w}{2}, \tag{77}$$

$$\int_{L-\frac{L_w}{2}}^{L} w_I(x)\left[\frac{d}{dx}\left\{\zeta_1 E\frac{d\hat{u}_H(x)}{dx}+\zeta_2\int_{-L_R}^{L-x}k(|\bar{x}|)E\frac{d\hat{u}_H(x+\bar{x})}{dx}\,d\bar{x}\right\}\right]dx$$
$$+\int_{L-\frac{L_w}{2}}^{L} w_I(x)\left[\frac{d}{dx}\left\{\zeta_1 E\frac{d\hat{u}_P(x)}{dx}+\zeta_2\int_{-L_R}^{L-x}k(|\bar{x}|)E\frac{d\hat{u}_P(x+\bar{x})}{dx}\,d\bar{x}\right\}+b(x)\right]dx$$
$$=0,\quad x_I=L. \tag{78}$$

In view of (18) and (26), the integrands of both integrals in (75) vanish. The remaining relations are thus those in (72)–(74) and (76)–(78). Integration by parts for (73), for instance, leads to

$$\int_{x_I-\frac{L_w}{2}}^{x_I+\frac{L_w}{2}}\frac{dw_I(x)}{dx}\left\{\zeta_1 E\frac{d\hat{u}_H(x)}{dx}+\zeta_2\int_{-x}^{L_R}k(|\bar{x}|)E\frac{d\hat{u}_H(x+\bar{x})}{dx}\,d\bar{x}\right\}dx$$
$$+\int_{x_I-\frac{L_w}{2}}^{x_I+\frac{L_w}{2}}\frac{dw_I(x)}{dx}\left\{\zeta_1 E\frac{d\hat{u}_P(x)}{dx}+\zeta_2\int_{-x}^{L_R}k(|\bar{x}|)E\frac{d\hat{u}_P(x+\bar{x})}{dx}\,d\bar{x}\right\}dx$$
$$-\int_{x_I-\frac{L_w}{2}}^{x_I+\frac{L_w}{2}} w_I(x)b(x)\,dx-w_I\left(x_I+\frac{L_w}{2}\right)\hat{\sigma}\left(x_I+\frac{L_w}{2}\right)$$
$$+w_I\left(x_I-\frac{L_w}{2}\right)\hat{\sigma}\left(x_I-\frac{L_w}{2}\right)=0,\quad \frac{L_w}{2}\leqslant x_I\leqslant L_R-\frac{L_w}{2}. \tag{79}$$

In the above relation $\hat{\sigma}(.)$ is the approximated stress at the point. Choosing a weight function so that $w_I(x_I+\frac{L_w}{2})=w_I(x_I-\frac{L_w}{2})=0$, see Fig. 3, the last two terms in (79) vanish and thus

$$\int_{x_I-\frac{L_w}{2}}^{x_I+\frac{L_w}{2}}\frac{dw_I(x)}{dx}\left\{\zeta_1 E\frac{du_H(x)}{dx}+\zeta_2\int_{-x}^{L_R}k(|\bar{x}|)E\frac{du_H(x+\bar{x})}{dx}\,d\bar{x}\right\}dx$$
$$=\int_{x_I-\frac{L_w}{2}}^{x_I+\frac{L_w}{2}} w_I(x)b(x)\,dx-f_P^I, \tag{80}$$

where f_P^I denotes the second integral in (79). For (72) or (78) in which the weight support intersects the boundary at $x=0$ or $x=L$ (e.g. a Neumann type) one may write (for (72))

$$\int_0^{L_w/2}\frac{dw_I(x)}{dx}\left\{\zeta_1 E\frac{du_H(x)}{dx}+\zeta_2\int_{-x}^{L_R}k(|\bar{x}|)E\frac{du_H(x+\bar{x})}{dx}\,d\bar{x}\right\}dx$$
$$=\int_0^{L_w/2} w_I(x)b(x)\,dx-w_I(0)\sigma(0)-f_P^I. \tag{81}$$

Note that in (81) we have replaced $\hat{\sigma}(0)$ with $\sigma(0)$ as a condition at $x=0$. A similar expression as (81) may be written for (78). Substitution of (19) in such relations results in a system of equations which may be written as

$$\mathbf{Kc}=\mathbf{F}. \tag{82}$$

In (82), $\mathbf{c}$ contains all coefficients as c_i in (19) and $\mathbf{F}$ contains all terms in the right hand side of the equations as in (80) and (81). Note that $\mathbf{K}$ is a rectangular matrix. The elements of $\mathbf{K}$, associated with the relation in (80), are as

$$k_{Ii}=\alpha_i\int_{x_I-\frac{L_w}{2}}^{x_I+\frac{L_w}{2}}\frac{dw_I(x)}{dx}\left\{\zeta_1 E+\zeta_2\int_{-x}^{L_R}k(|\bar{x}|)Ee^{\alpha_i\bar{x}}\,d\bar{x}\right\}e^{\alpha_i x}dx. \tag{83}$$

The elements associated with other relations pertaining to (74), (76), and (77) are found in an analogous manner. The readers may also note that we have started with assuming that L_R is discretized by a number of cells with equal sizes (and the discretization is continued till one cell beyond L_R) so that the width of the boundary layer zone becomes $L_R+L_w/2$. In the case of using cells with unequal sizes the bounds of the integrals and the boundary layer zone may be defined by analogy.

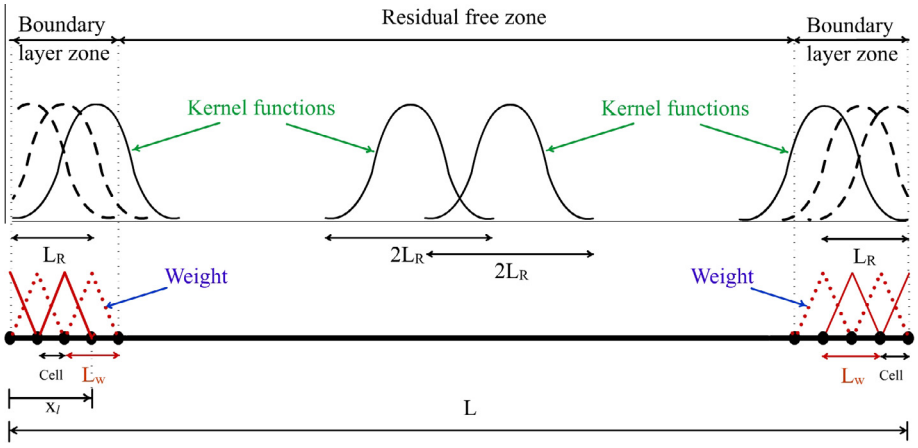

Fig. 3. Schematic presentation of the boundary layer zone defined by the kernel function and the cell size.

Remark 3. In the case that the kernel function is defined on an unbounded support/domain, i.e. $L_R \to \infty$, the integrands in (75) do not vanish. This leads to additional relations in (82). The elements of **K** for such cases are written as

$$k_{Ii} = \alpha_i \int_{x_I - \frac{L_w}{2}}^{x_I + \frac{L_w}{2}} \frac{dw_I(x)}{dx} \left\{ \zeta_1 E + \zeta_2 \int_{-x}^{L-x} k(|\bar{x}|) E e^{\alpha_i \bar{x}} \, d\bar{x} \right\} e^{\alpha_i x} dx. \tag{84}$$

The elements of **F** may be found by analogy. In practice there is no need for considering such relations in zones far from the boundaries because in the central zones the residuals are considerably small.

Remark 4. The matrix **K** and the array **F** in (82) may be constructed by an assembly process when the weight functions w_I are locally defined on a mesh of cells/elements. We call such a mesh as the "weight mesh" hereafter. However, the assembly process is just performed on the rows of **K** or **F** (since the EBFs are defined over the whole computational domain). Obviously the matrix relation for each cell depends on the location of the cell in the domain. For instance for a generic cell with linear variation of the weight, falling in a region that (83) is valid as shown in Fig. 3, the contribution of the cell to the arrays **K** and **F** is written as

$$k^e_{mi} = \alpha_i \int_{x^e_1}^{x^e_2} \frac{dN^e_m}{dx} \left\{ \zeta_1 E + \zeta_2 \int_{-x}^{L_R} k(|\bar{x}|) E e^{\alpha_i \bar{x}} \, d\bar{x} \right\} e^{\alpha_i x} dx, \quad m = 1, 2, \tag{85}$$

and

$$F^e_{mi} = \int_{x^e_1}^{x^e_2} N^e_m b(x) \, dx - \sum_r h_r \alpha_r \int_{x^e_1}^{x^e_2} \frac{dN^e_m}{dx} e^{\alpha_r x} \times \left\{ \zeta_1 E + \zeta_2 \int_{-x}^{L_R} k(|\bar{x}|) E e^{\alpha_r \bar{x}} \, d\bar{x} \right\} dx \quad m = 1, 2. \tag{86}$$

In the above relations N^e_m represents the cell/element shape functions, used as the weight, while x^e_1 and x^e_2 are the coordinates of the two ends. The above relations are associated to (73) which is valid for the interval of $0 \leqslant x_I \leqslant L_R - \frac{L_w}{2}$. The readers may note that when similar relations associated to (74), which is valid for the interval of $L_R - \frac{L_w}{2} < x_I < L_R + \frac{L_w}{2}$, are of concern and when a boundary layer mesh is to be used for cells with $L_R < x^e_1 < L_R + \frac{L_w}{2}$, just one of the relations, i.e. for $m = 1$, is taken into account for the assembly process.

One remaining point is concerning with the satisfaction of the boundary conditions. It is clear that Neumann conditions appear in **F** as in the second term in the right hand side of (81). However, Dirichlet conditions do not appear straightforwardly in (82). To satisfy such conditions we use a collocation approach. For instance when a condition as $u(0) = u_0$ is of concern we write

$$\hat{u}|_{x=0} = u_0. \tag{87}$$

Now in view of (30) the following relation may be written

$$\left[\sum_i c_i e^{\alpha_i x} + \sum_r h_r e^{\alpha_r x} \right]_{x=0} = u_0. \tag{88}$$

This leads to a new relation for the coefficients c_i as

$$\sum_i c_i = u_0 - \sum_r h_r, \tag{89}$$

which may be included in the matrix relation in (82). We find the values of c_i by the procedure explained in Appendix A.

5.2. Two-dimensional problems

The formulation given for the 1D problems may be easily extended to the 2D problems. A weighted residual expression is written as

$$\int_\Omega \mathbf{w}_I \left(\mathbf{S}^T \left\{ \zeta_1 \mathbf{D}\mathbf{S}\hat{\mathbf{u}}(\mathbf{x}) + \zeta_2 \int_{\Omega_s} k(|\bar{\mathbf{x}}|) \mathbf{D}\mathbf{S}\hat{\mathbf{u}}(\mathbf{x} + \bar{\mathbf{x}}) \, d\Omega_s \right\} + \mathbf{b} \right) d\Omega = 0, \quad \mathbf{w}_I = w_I \mathbf{I}. \tag{90}$$

In the definition of $\mathbf{w}_I$ in (90) $\mathbf{I}$ is a 2×2 identity matrix. The weight function w_I is defined on a compact support as Ω_w

$$\begin{cases} w_I \neq 0 & \mathbf{x} \in \Omega_w, \\ w_I = 0 & \mathbf{x} \notin \Omega_w. \end{cases} \tag{91}$$

In view of (55) and (91) one may rewrite (90) as

$$\int_{\Omega_w} \mathbf{w}_I \left(\mathbf{S}^T \left\{ \zeta_1 \mathbf{D}\mathbf{S}\hat{\mathbf{u}}_H(\mathbf{x}) + \zeta_2 \int_{\Omega_s} k(|\bar{\mathbf{x}}|) \mathbf{D}\mathbf{S}\hat{\mathbf{u}}_H(\mathbf{x} + \bar{\mathbf{x}}) \, d\Omega_s \right\} \right) d\Omega_w + \int_{\Omega_w} \mathbf{w}_I \left(\mathbf{S}^T \left\{ \zeta_1 \mathbf{D}\mathbf{S}\hat{\mathbf{u}}_P(\mathbf{x}) + \zeta_2 \int_{\Omega_s} k(|\bar{\mathbf{x}}|) \mathbf{D}\mathbf{S}\hat{\mathbf{u}}_P(\mathbf{x} + \bar{\mathbf{x}}) \, d\Omega_s \right\} \right) d\Omega_w + \int_{\Omega_w} \mathbf{w}_I \mathbf{b} \, d\Omega_w = 0. \tag{92}$$

By assuming that Ω_w is much smaller than the main computational domain Ω, the relation in (92) may be written for two regions Ω_b and Ω_0

$$\Omega = \Omega_b \cup \Omega_0, \tag{93}$$

where Ω_b is a boundary layer region defined within a distance of $L_R + \kappa L_w$ $(0 \leqslant \kappa \leqslant 1)$ from the boundary $\Gamma = \Gamma_u \cup \Gamma_t$, and Ω_0 repre-

sents the rest of the domain. Here L_w is the diameter of Ω_w measured along the normal to the boundary. Similar to (75) for one-dimensional problems, the integrands in (92) vanish when Ω_w completely falls inside Ω_0. Therefore (92) must be written when Ω_w falls inside Ω_b.

As in 1D problems, in practice we construct a 2D mesh for defining the weight functions (see Remark 4). Relation (92) is written for all weight functions defined on the nodes (hat functions). With all such relations a system of equations, as in (82), is resulted. When an integration by part is used the elements of $\mathbf{K}$ take the following form

$$(\mathbf{k}_{li})_{2\times 2} = \int_{\Omega_w} [\mathbf{Sw}_l]^T \left\{ \zeta_1 \mathbf{DSh}^i + \zeta_2 \int_{\Omega_s} k(|\bar{\mathbf{x}}|) \mathbf{DSh}^i e^{\alpha_i \bar{x} + \beta_i \bar{y}} \, d\Omega_s \right\} e^{\alpha_i x + \beta_i y} \, d\Omega_w. \quad (94)$$

By writing the relations at the cell/element level, when the element shape functions are considered as the weights, one may employ an assembly procedure to construct the system of equations. The assembly of such relation leads to a system of equations as in (82). For linear rectangular elements, for instance, when the cell is in Ω_b, one may write

$$(\mathbf{k}^e_{mi})_{2\times 2} = \int_{\Omega_e} [\mathbf{SN}^e_m]^T \left\{ \zeta_1 \mathbf{DSh}^i + \zeta_2 \int_{\Omega_s} k(|\bar{\mathbf{x}}|) \mathbf{DSh}^i e^{\alpha_i \bar{x} + \beta_i \bar{y}} \, d\Omega_s \right\} e^{\alpha_i x + \beta_i y} \, d\Omega_e, \quad m = 1, \ldots, 4, \quad (95)$$

and

$$\mathbf{F}^e_{mi} = -\sum_{r,s} \left\{ \int_{\Omega_e} [\mathbf{SN}^e_m]^T \left\{ \zeta_1 \mathbf{DSh}_{rs} + \zeta_2 \int_{\Omega_s} k(|\bar{\mathbf{x}}|) \mathbf{DSh}_{rs} e^{\alpha_r \bar{x} + \beta_s \bar{y}} \, d\Omega_s \right\} e^{\alpha_r x + \beta_s y} \, d\Omega_e \right\} + \int_{\Omega_e} \mathbf{N}^e_m \mathbf{b} \, d\Omega_e + \int_{\Gamma_e} \mathbf{N}^e_m \mathbf{t} \, d\Gamma. \quad (96)$$

In the above relations Ω_e and Γ_e denote the cell area and its boundary, respectively. Also $\mathbf{N}^e_m = N^e_m \mathbf{I}$ in which N^e_m is the m th shape function of the cell. The last term in the right hand side of (96) is taken into account when the cell is adjacent to the boundary with Neumann conditions.

In order to include Dirichlet conditions, similar to the 1D cases, we use a collocation approach. To this end, in view of (2) and (55), we write

$$\hat{\mathbf{u}}_H + \hat{\mathbf{u}}_P = \mathbf{u}_B \text{ on } \Gamma_u. \quad (97)$$

This leads to a new set of equations in terms of the coefficients c_i as

$$\sum_i c_i \mathbf{h}^i e^{\alpha_i x_B + \beta_i y_B} = \mathbf{u}_B - \sum_{r,s} \mathbf{h}_{rs} e^{\alpha_r x_B + \beta_s y_B} \quad (x_B, y_B) \in \Gamma_u, \quad (98)$$

which is included in the system of equations to be solved. For the sake of conciseness we shall not present the details of the formulation since one may follow it with a rationale similar to that used in 1D problems.

6. Numerical experiments

In this section we present the results of our numerical experiments on 1D and 2D problems.

6.1. One-dimensional problems

We consider determinate as well as indeterminate 1D problems as shown in Fig. 4. In order to present the results we use the following normalized strain field

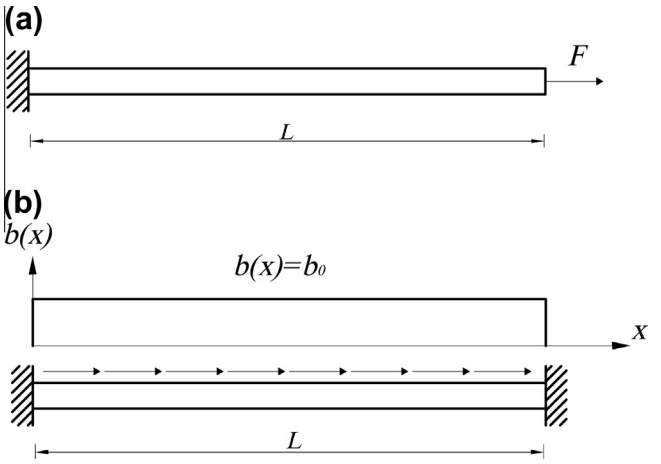

Fig. 4. Loading conditions for nonlocal elastic bar: (a) end concentrated force; (b) constant body force.

$$\bar{\varepsilon} = \frac{EA}{\bar{F}} \hat{\varepsilon}, \quad \bar{F} = \int_0^L |b(x)| \, dx + |F_L|, \quad (99)$$

where $|F_L|$ denotes the magnitude of the force at the end of the bar in the determinate problems. For the indeterminate problems we use $F_L = 0$. Also in (99), $b(x)$ denotes the body force of the problem.

To give an insight to the accuracy of the solution in the determinate problems we define the following norm

$$\eta_\sigma = \left(\frac{\int_\Omega R_\sigma^2 \, d\Omega}{\int_\Omega \sigma^2 \, d\Omega} \right)^{1/2}, \quad (100)$$

in which

$$R_\sigma(x) = \sigma(x) - \left[\zeta_1 E \hat{\varepsilon}(x) + \zeta_2 \int_0^L k(|x' - x|) E \hat{\varepsilon}(x') \, dx' \right]. \quad (101)$$

Moreover, in order to compare the results with those from other references, we define the following norm

$$\bar{\eta} = \left(\frac{\sum_{i=1}^{NP} (\varepsilon_1(x) - \varepsilon_2(x))^2}{\sum_{i=1}^{NP} (\varepsilon_2(x))^2} \right)^{1/2}, \quad (102)$$

in which $\varepsilon_1(x)$ and $\varepsilon_2(x)$ are two strain fields obtained from two solution methods. In the above relation NP is the number of points selected inside the domain (for instance $NP = 1000$).

To begin with, we present the results for the solution of the determinate bar shown in Fig. 4a solved with the use of the EBFs and a set of cells defined over the boundary layer zone. The kernel function is as the one given in (56). For this problem, a closed form

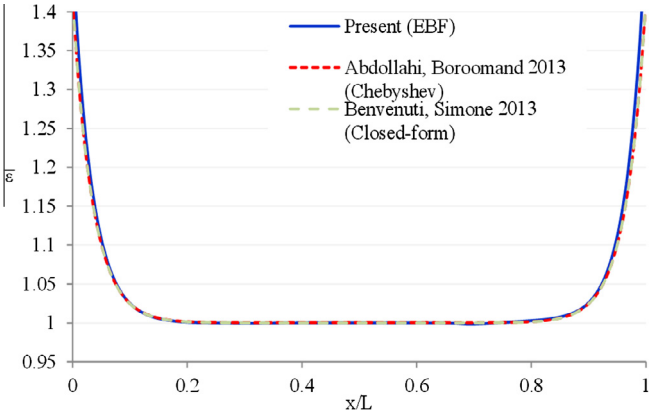

Fig. 5. Comparison of the results obtained for 1D determinate bar in Fig. 4a.

Table 1
The error norms for different number of EBFs and cells in the solution of determinate bar.

No. of bases	No. of cells	η_σ	$\bar{\eta}$
34	52	0.00128	0.00138
42	202	0.00105	0.00107
62	202	0.00059	0.00061

solution has recently been presented by Benvenuti and Simone (2013) for $L_R \to \infty$. Recalling that for $L_R \to \infty$ the kernel in (56) does not generate enough number of EBFs (see (58)), for the validation of the results, we solve the problem by relatively large L_R, as $L_R/l = 7$, and find the roots of (22) numerically to construct the EBFs. The final results are then compared with the closed form solution (in this example $\zeta_1/\zeta_2 = 1$ and $l = L/20$). 66 EBFs and 202 cells are used for the solution. Fig. 5 depicts the results obtained for $\bar{\varepsilon}$. We have included the results obtained by the Chebyshev series presented by Abdollahi and Boroomand (2013). Excellent agreement is observable in the results.

We further perform a convergence study and solve the problem with different numbers of EBFs and cells. Since the closed form solution given by Benvenuti and Simone (2013) is just for the case of $L_R \to \infty$, we consider the results obtained by Chebyshev series in our latest studies (for $L_R/l = 5$) as the reference solution for comparisons. Again a set of cells with equal lengths are used. Table 1 shows the error norm evaluated for different numbers of EBFs and cells used. For each case we have evaluated the deviation of the strains from those recently reported by the authors (Abdollahi and Boroomand, 2013) using Chebyshev polynomials. As is seen, the error norm decreases when the number of EBFs grows. Moreover, both error norms η_σ and $\bar{\eta}$ follow each other. This is because the solution obtained in the previous study is of very low residual and thus it is very close to the exact solution.

In order to give some insight to the concept of boundary layer method proposed in this paper, we repeat the solution with a non-uniform distribution of the cells. Fig. 6(a) depicts a sample of the cell configurations used. As is seen we have used a set of cells arranged just near the two ends (see Fig. 6(b) for the distribution of the cell length along the bar). Table 2 contains the results obtained for η_σ while $l = L/20$ and for different values of L_R/l (for bounded kernels). For $L_R/l = 5$ one may compare the results with those reported in Table 1. It can clearly be seen that by using less number of elements just near the two ends one may still obtain results with excellent accuracy.

We repeat the solution using the kernel function defined in (57). To generate the EBFs we use (63) given for the cases in which $L_R \to \infty$. We first use a set of cells with equal lengths covering the whole computational domain. Table 3 reports the norms η_σ, see (100), obtained for different numbers of cells and EBFs. As is seen the error monotonically decreases when the number of EBFs grows. Note that there is no reference result in the literature, using the kernel in (57), for calculating the error of strains. We repeat the solution with a non-uniform distribution of the cells. Fig. 6(c) depicts a sample of the cell configurations used. The results are reported in the same table. It can be observed that with less number of cells one can obtain results with less error.

Fig. 7 shows the normalized strain fields for different values of l and ζ_1/ζ_2 for the kernel function defined in (57). The strain fields may be compared with those given in the previous research by the authors (Abdollahi and Boroomand, 2013) for the kernel defined in (56). In the same line, the readers may refer to the studies by Benvenuti and Tralli (2006) for the results of FEM using fast Gauss transform.

As another case for 1D problems, the indeterminate problem of Fig. 4b is considered. Here again the kernel function is as the one given in (56) with bounded domain ($L_R/l = 5$). In the recent studies by the authors (Abdollahi and Boroomand, 2013), the problem has been solved using a superposition approach from the results obtained for determinate problem. Note that when using the EBFs,

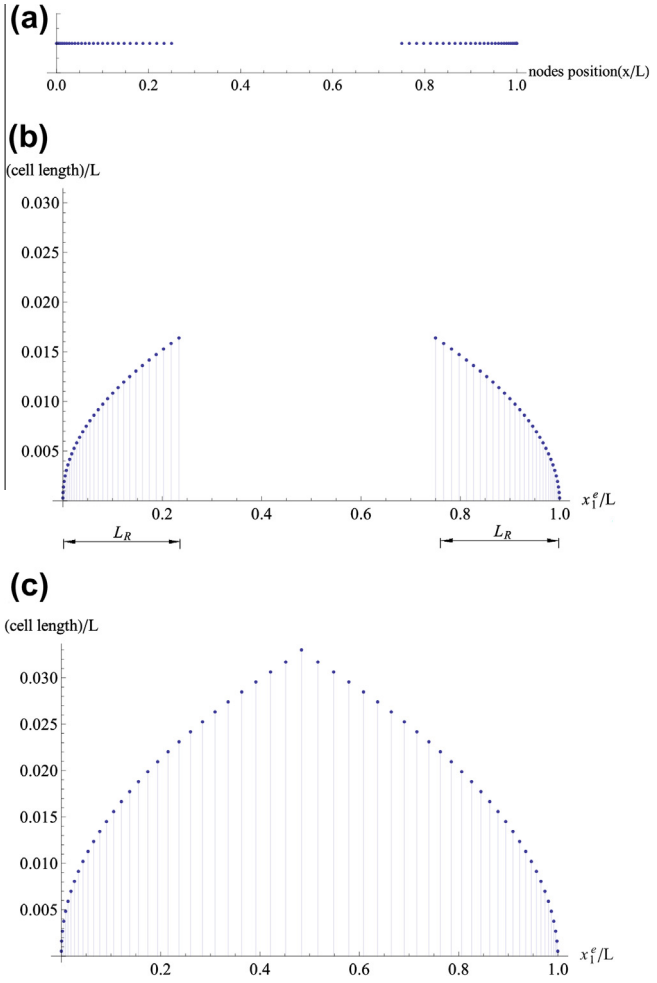

Fig. 6. Cell configurations (61 cells): (a) the position of nodes on the bar, (b) the distribution of the cell length along the bar for bounded kernels and for $L_R/l = 5$ and $l = L/20$, (c) the distribution of the cell length along the bar for unbounded kernels.

Table 2
The error norms for different number of EBFs for cell configurations as the one shown in Fig. 6(b).

L_R/l	No. of bases	η_σ
5	42	0.000828
4	42	0.001693
3	22	0.007821

Table 3
The error norms for different number of EBFs using the kernel function defined in (57).

No. of bases	Cells with equal lengths		Cell configuration as Fig. 6(c)	
	No. of cells	η_σ	No. of cells	η_σ
20	200	2.88 E−5	61	3.78E−5
24	200	9.13E−6	61	6.28E−6
28	200	6.54E−6	61	1.02E−6

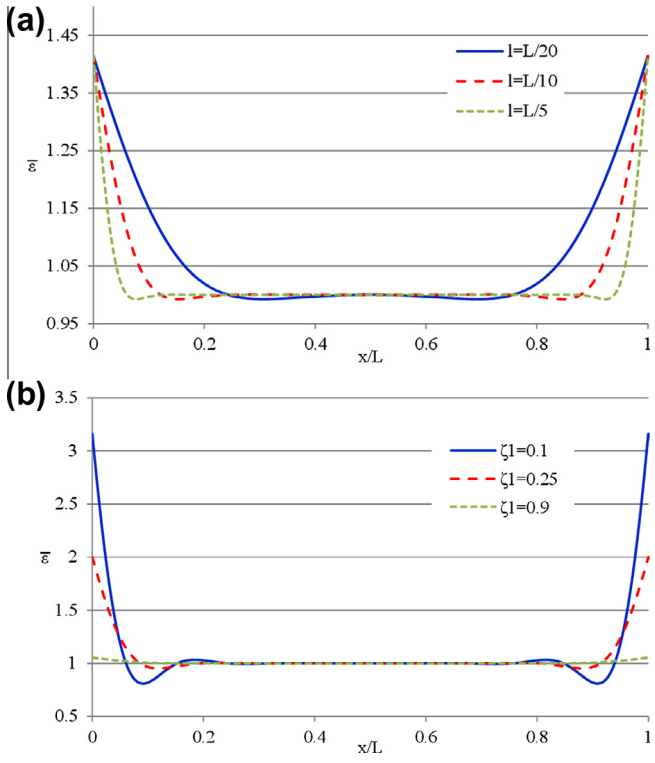

Fig. 7. Normalized strain fields obtained for bar of Fig. 4(a): (a) for $\zeta_1/\zeta_2 = 1$ and for different values of l (b) for $l = L/20$ and for different values of ζ_1.

one can directly solve the problem by considering the boundary conditions at the two ends. Fig. 8 demonstrates that the results of the current analysis coincide with those reported by the authors (Abdollahi and Boroomand, 2013). In Fig. 9 we report the results of the method when using the kernel function defined in (57) for different values of l and ζ_1/ζ_2. Table 4 reports the results of this case obtained for η_σ while $l = L/20$, $\zeta_1/\zeta_2 = 1$ and cell configuration shown in Fig. 6(c). In obtaining the results with body force, we have used a number of EBFs, see (27), constructed by considering $\alpha_r = \mathbf{i}r\Delta\bar{b}$, $\Delta\bar{b} \in \mathbb{R}^+$, and $r \in \{-N_r, ..., -1, 0, 1, ..., N_r\}$ fitted on a number of values on some sampling points (denoted by P) to express the body force (the values of $\Delta\bar{b}$, N_r and P are shown in Table 4).

6.2. Two-dimensional problems

Here again, to give an insight to the accuracy of the solution, the following residuals are defined

$$\mathbf{R}_\Omega = \mathbf{S}^T\hat{\boldsymbol{\sigma}} + \mathbf{b} \quad \text{in } \Omega, \tag{103}$$

and

$$\mathbf{R}_\Gamma = \tilde{\mathbf{n}}\hat{\boldsymbol{\sigma}} - \mathbf{t} \quad \text{on } \Gamma_t, \tag{104}$$

and based on such residuals we define the following norms

$$\|\mathbf{R}_\Omega\| = \left(\int_\Omega \mathbf{R}_\Omega^T\mathbf{R}_\Omega d\Omega\right)^{1/2} \quad \text{and} \quad \|\mathbf{R}_\Gamma\| = \left(\int_\Gamma \mathbf{R}_\Gamma^T\mathbf{R}_\Gamma d\Gamma\right)^{1/2}. \tag{105}$$

However the difficulty is that they are not dimensionless and thus the estimation of their largeness/smallness is not an easy task. One may compare the residual norms with the norm of the prescribed values; for instance $\|\mathbf{R}_\Omega\|$ and $\|\mathbf{R}_\Gamma\|$ may be compared with $\|\mathbf{b}\|$ and $\|\mathbf{t}\|$, respectively. Thus the following normalized norm may be found useful

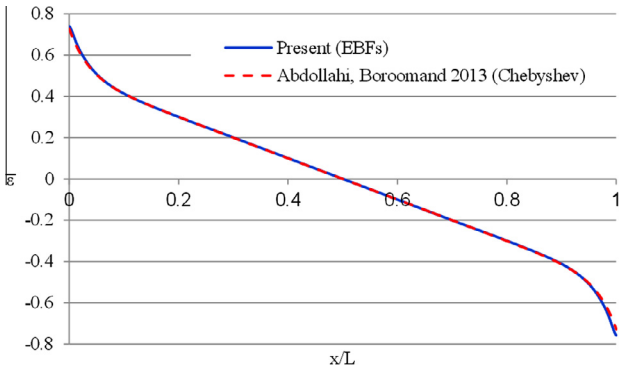

Fig. 8. Normalized strain fields obtained for indeterminate bar of Fig. 4(b) for $l = L/20$, $\zeta_1/\zeta_2 = 1$ using the kernel in (56).

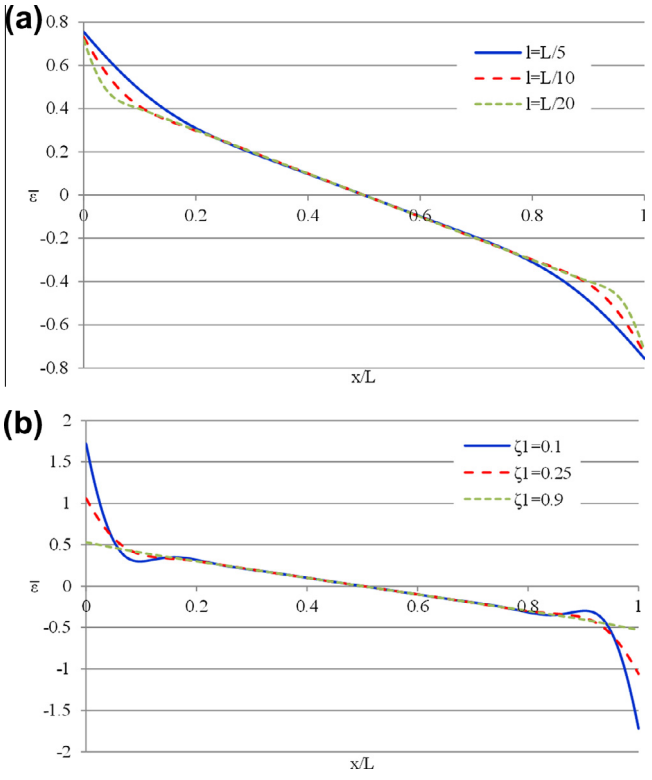

Fig. 9. Normalized strain fields obtained for indeterminate bar of Fig. 4(b) using the kernel in (57): (a) for $\zeta_1/\zeta_2 = 1$ and for different values of l (b) for $l = L/20$ and for different values of ζ_1.

$$\eta = \frac{\sqrt{A_\Omega}\|\mathbf{R}_\Omega\| + \sqrt{L_\Gamma}\|\mathbf{R}_\Gamma\|}{\sqrt{A_\Omega}\|\mathbf{b}\| + \sqrt{L_\Gamma}\|\mathbf{t}\|}, \quad \|\mathbf{t}\| = \left(\int_\Gamma \mathbf{t}^T\mathbf{t} d\Gamma\right)^{1/2},$$
$$\|\mathbf{b}\| = \left(\int_\Omega \mathbf{b}^T\mathbf{b} d\Omega\right)^{1/2}. \tag{106}$$

In the above relation A_Ω is the area occupied by the 2D domain Ω and L_Γ is the total length of its boundary $\Gamma \equiv \partial\,\Omega$. For problems with no body force one may use an appropriate scale of $\|\mathbf{t}\|$ for the equilibrium residuals. For such cases we define the following norm as an error indicator (see also Abdollahi and Boroomand, 2013)

$$\eta = \frac{\sqrt{A_\Omega}\|\mathbf{R}_\Omega\| + \sqrt{L_\Gamma}\|\mathbf{R}_\Gamma\|}{2\sqrt{L_\Gamma}\|\mathbf{t}\|}. \tag{107}$$

Table 4
The error norms for different number of EBFs for cell configuration shown in Fig. 6(c) using the kernel function defined in (57) with unbounded domain and $l = L/20$, $\zeta_1/\zeta_2 = 1$.

No. of bases for homogeneous part	Parameters used for particular solution			η_Ω
	$\Delta\bar{b}$	N_r	P	
20	0.02	5	10	6.68E−5
24	0.02	5	10	1.69E−5
28	0.02	5	10	6.56E−6

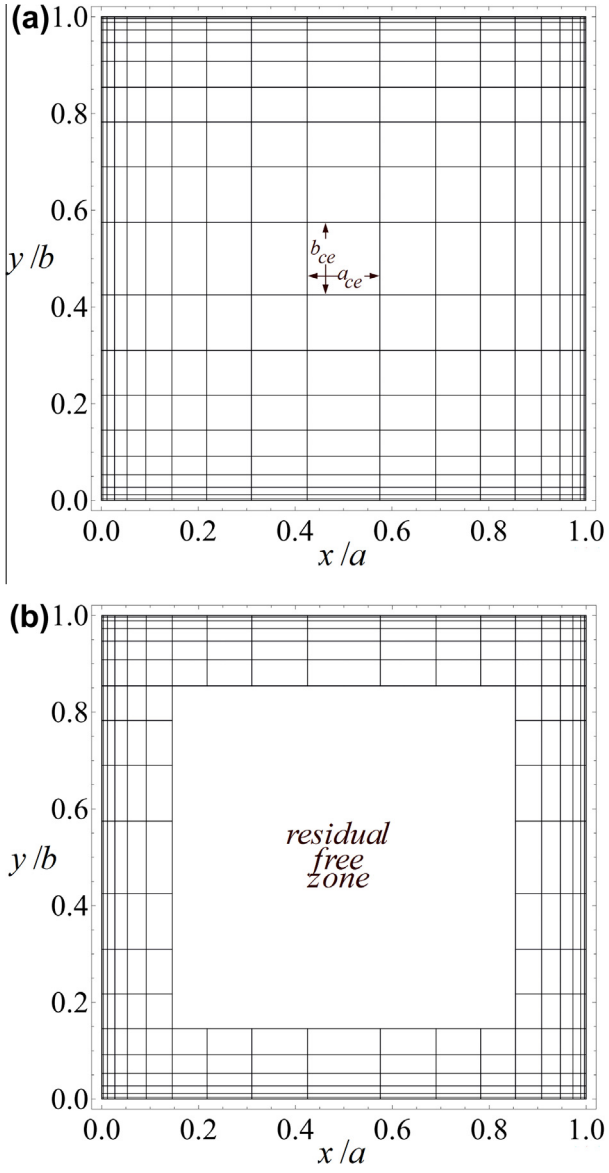

Fig. 10. 2D cell configurations ($a_{ce} = b_{ce} = 0.15L$, 21×21cells): (a) for unbounded kernels; (b) for bounded kernel and for $L_R/l = 2$ and $l = L/20$.

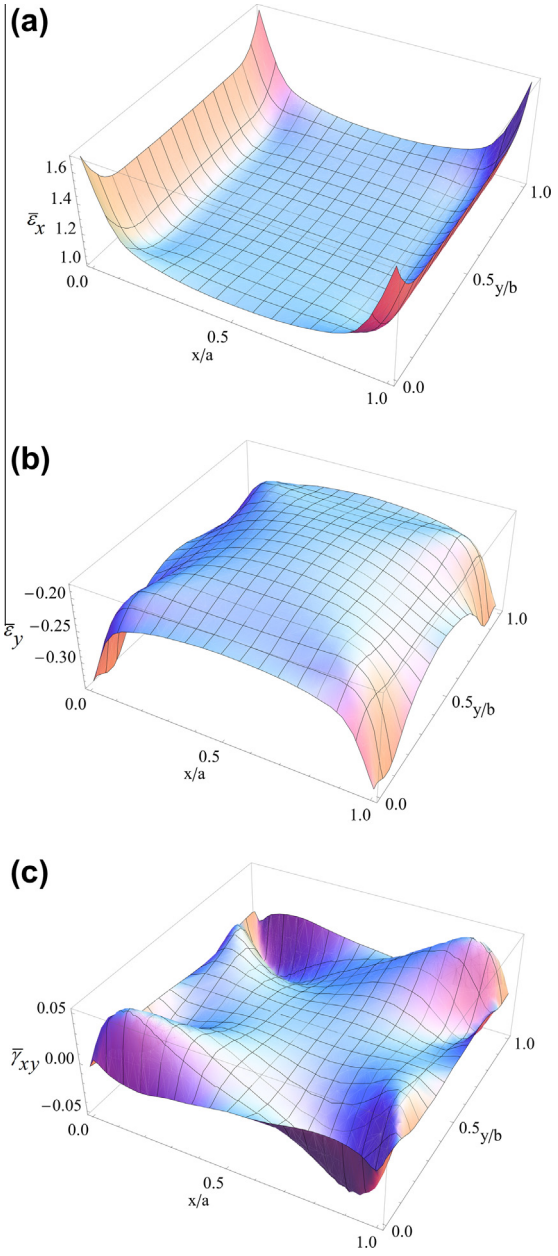

Fig. 11. Distribution of the normalized strains in the 2D benchmark solved with $a_{ce} = b_{ce} = 0.15L$; (a) distribution of $\bar{\varepsilon}_x$ (b) distribution of $\bar{\varepsilon}_y$, (c) distribution of $\bar{\gamma}_{xy}$.

Table 5
The error norms for different cell configurations using the unbounded kernel function for $l = L/10$, $\zeta_1/\zeta_2 = 1$ and mesh configurations as Fig. 10(a).

Classical bases	Eq. (40) bases	$a_{ce} = b_{ce}$	No. of elements	η	$\bar{\eta}$
144	36	$0.15L$	21×21	0.0177	0.0163
144	36	$0.25L$	21×21	0.0179	0.0164
144	36	$0.35L$	21×21	0.0182	0.0167
144	36	$0.45L$	21×21	0.0190	0.0171

Furthermore, in order to compare the results with those from other references, we define the following norm

$$\bar{\eta} = \left(\frac{\sum_{i=1}^{NP} (\boldsymbol{\varepsilon}_1 - \boldsymbol{\varepsilon}_2)^T (\boldsymbol{\varepsilon}_1 - \boldsymbol{\varepsilon}_2)}{\sum_{i=1}^{NP} \boldsymbol{\varepsilon}_2^T \boldsymbol{\varepsilon}_2} \right)^{1/2}, \tag{108}$$

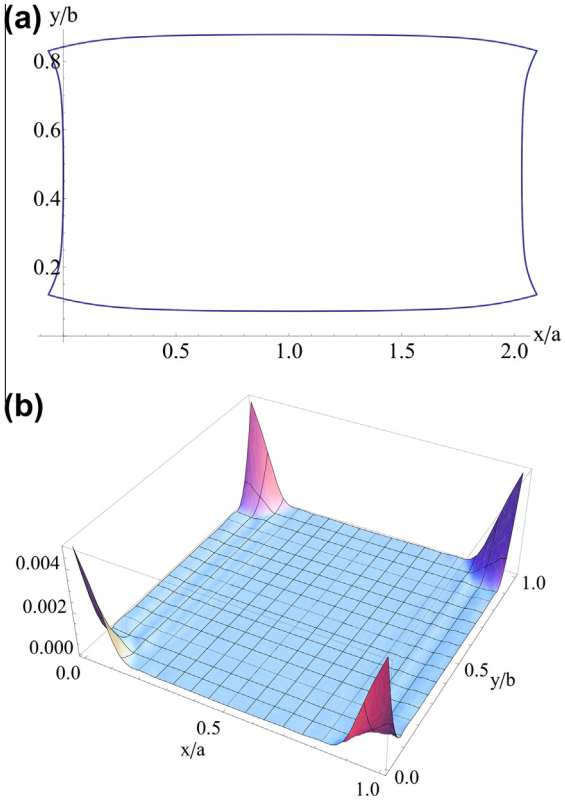

Fig. 12. (a) Magnified deformed shape of the domain obtained by $x/a+\bar{u}$ and $y/b+\bar{v}$, (b) distribution of $\sqrt{A_\Omega}\sqrt{\mathbf{R}_\Omega^T\mathbf{R}_\Omega}/\sqrt{L_\Gamma}\|\mathbf{t}\|$.

in which $\boldsymbol{\varepsilon}_1$ and $\boldsymbol{\varepsilon}_2$ are two strain fields obtained from two solution methods. In the above relation NP is the number of points selected inside the domain (for instance $NP = 10000$).

We consider a square domain $0 \leqslant x \leqslant L$, $0 \leqslant y \leqslant L$ (or $a = b = L$). The Young's modulus and the Poisson's ratio are considered as; E and $\nu = 0.2$ respectively. We present the solution of the problem under plane stress conditions with $\zeta_1 = \zeta_2 = 0.5$. The following normalized displacement, strain and stress fields are defined for the presentation of the results:

$$\bar{\mathbf{u}} = \frac{E}{\bar{t}L}\hat{\mathbf{u}}, \quad \bar{\boldsymbol{\varepsilon}} = \frac{E}{\bar{t}}\hat{\boldsymbol{\varepsilon}}, \quad \bar{\boldsymbol{\sigma}} = \frac{1}{\bar{t}}\hat{\boldsymbol{\sigma}}, \quad \bar{t} = |\sigma_0|, \tag{109}$$

where $|\sigma_0|$ denotes the magnitude of the tractions defined in each problem. To generate the EBFs, pertaining to the characteristic equation (40), we solve (67) given for the cases in which $L_R \to \infty$. We consider the roots for α when $\beta_i = 0$ and those for β when $\alpha_i = 0$. According to Remark 3 there is no need to considering a large number of cells in the central zone of the domain. Therefore we use a cell configuration including a large cell in the center ($a_{ce} \times b_{ce}$) and for the boundary effect we arrange the cells in a boundary layer. The cell sizes decrease quadratically towards the boundaries (unidirectionally near the edges and bidirectionally at corners). Fig. 10(a) shows a sample of cell configurations used.

To being with, we present the results for the solution of a problem with equilibrated tractions as

$$\mathbf{t}|_{x=0,y} = \langle -\sigma_0, 0\rangle^T, \quad \mathbf{t}|_{x=L,y} = \langle \sigma_0, 0\rangle^T, \quad \mathbf{t}|_{x,y=0} = \mathbf{t}|_{x,y=L} = \mathbf{0}, \tag{110}$$

with σ_0 being the magnitude of the tractions. The Dirichlet boundary conditions (least supports) are defined as

$$u|_{x=0,y=L/2} = v|_{x=0,y=L/2} = 0, \quad v|_{x=L,y=L/2} = 0. \tag{111}$$

Table 6
The error norms for different values of L_R/l and l/L using the bounded kernel function $\zeta_1/\zeta_2 = 1$.

l/L	L_R/l	Classical bases	Eq. (40) bases	No. of elements	η
1/10	2	144	36	416	0.0192
1/10	3	144	36	432	0.0178
1/20	2	144	28	392	0.0217
1/20	3	144	28	416	0.0205

Table 7
The error norms for $l = L/10$ and for different values of L_R/l using the bounded kernel function $\zeta_1/\zeta_2 = 1$.

L_R/l	Classical bases	Eq. (40) bases	No. of elements	η
2	144	36	416	0.0187
3	144	36	432	0.0179

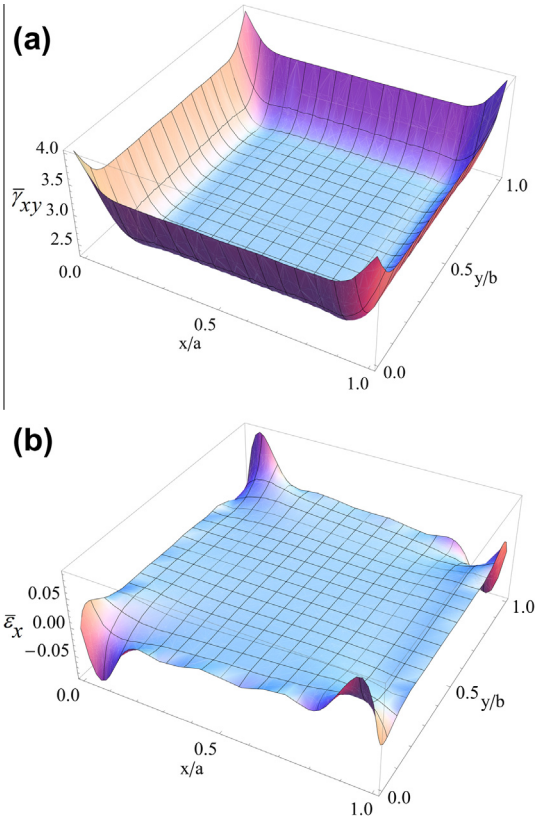

Fig. 13. Distribution of the normalized strains in the 2D problem with shear tractions; (a) distribution of $\bar{\gamma}_{xy}$, (b) distribution of $\bar{\varepsilon}_x$.

Table 5 shows the error norms evaluated for different cell configurations used. For each case we have evaluated the deviation of the strains from those recently reported by the authors (Abdollahi and Boroomand, 2013) using Chebyshev polynomials. The results reported for $\bar{\eta}$ in Table 5 show such a deviation between the two solutions. The readers may note that although η and $\bar{\eta}$ are obtained within a rather similar order, we do not expect that they vary similarly since the reference solution used still has a small error and does not play the role of a perfect exact solution (the error reported by Abdollahi and Boroomand, 2013 is $\eta = 0.00734$). It can be seen that while the error norms are reasonably low in all cases, they do not significantly grow by increasing the size of the central cell. This shows that one may effectively use a boundary layer mesh.

Fig. 11 depicts the distribution of strain components obtained with $a_{ce} = b_{ce} = 0.15L$. The strain field obtained may be compared with that evaluated in our previous work (2013). It may suffice to mention that the computational time of the presented results in this paper is approximately two logarithmic order of magnitude less than the time consumed for the solution using Chebyshev polynomials (e.g. compared with the case that 169 Chebyshev polynomials are used for the solution). The readers may also refer to the studies by Zingales et al. (2011) for a rather similar strain distribution obtained by FEM and using a 2D kernel analogous to (56). Fig. 12 shows the magnified deformed shape of the domain (obtained by $x/a + \bar{u}$ and $y/b + \bar{v}$) and the residual distribution corresponding to the first row of Table 6.

We repeat the solution again with the kernel function defined on unbounded domains (see (66) for the characteristic function). However, in the evaluation of the integrals we truncate the integrands when the kernel is to be evaluated for distances more than L_R. Therefore, the bases and the cell configurations are the same as those used previously but we ignore the cells in the low residual zone (i.e. the zone which could be considered residual free when the bounded kernel would be used). Fig. 10(b) shows a sample of cell configuration used for $L_R/l = 2$ and $l = L/20$. For the construction of such a cell distribution we simply remove those cells in Fig. 10(a) which fall in the residual free (low residual) zone. The results are reported in Table 6. As is seen again, the order of the errors norms is rather similar to the order of the errors reported in Table 5. The results of Tables 5 and 6 show that the kernel function defined on unbounded domain (see (66)) may serve as an effective tool for simplifying the solution process.

We also present the results for the solution of a problem with shear tractions defined as

$$\mathbf{t}|_{x=0,y} = \langle 0, -\sigma_0 \rangle^T, \quad \mathbf{t}|_{x=L,y} = \langle 0, \sigma_0 \rangle^T, \quad \mathbf{t}|_{x,y=0} = \langle -\sigma_0, 0 \rangle^T, \quad \mathbf{t}|_{x,y=L} = \langle \sigma_0, 0 \rangle^T. \tag{112}$$

The Dirichlet boundary conditions (least supports) are defined as

$$u|_{x=0,y=0} = v|_{x=0,y=0} = 0, \quad u|_{x=L,y=L} = v|_{x=L,y=L} \neq 0. \tag{113}$$

Table 7 contains the values of η obtained for this case using the unbounded kernel and the same bases and cell configurations as the previous case. Fig. 13(a) and (b) show the distribution of the normalized strain components ($\bar{\gamma}_{xy}$ and $\bar{\varepsilon}_x$) obtained for this load case.

7. Conclusions

In this paper we have presented exponential bases functions (EBFs) for nonlocal elasticity integral problems defined on unbounded domains. The EBFs play the role of fundamental solutions and may be used to reduce the discretization labor as in the methods using boundary elements/nodes. It has been shown that the EBFs obtained for the classical theory satisfy the equilibrium equations of the nonlocal theory regardless of the type of the kernel/attenuation function. It has also been shown that there exist some additional EBFs which depend on the type of the kernel/attenuation function used. These additional EBFs are the results of an additional characteristic equation which appear just in nonlocal elasticity theory. For further use we have presented the roots of such characteristic equations for 1D problems. For 2D problems, we have presented a simple characteristic equation, for unbounded kernels, which can be solved straightforwardly. With the EBFs in hand we have proposed a boundary layer method in order to use the EBFs, obtained for unbounded domains, in the solution of problems defined on bounded domains. Through a weighted residual approach we have shown that the solution just needs a series of cells near the boundaries for defining the weight functions. We have demonstrated the capabilities of the method in the solution of some 1D/2D problems. Although we have not explicitly compared the computational cost of the method with that of the existing ones, it is expected that the difference between the computational time of the proposed method and that of FEM be rather similar to the difference between the cost of the BEM and FEM especially when the length of nonlocal effect is sufficiently small in comparison with the size of the main computational domain. Of course this effect becomes more important when 3D problems are of concern.

The method we presented in this paper can straightforwardly be applied to the solution of plate bending problems using Eringen's integral. In this regard, the well-known plate theories may be used to reduce the general 3D model to a 2D one; however, before doing so the validity of the assumptions for the through-thickness variation of the strains and the suitability of the definition of the boundary conditions should be examined. This may be performed by testing the validity of the assumptions in converting a 2D problem to a 1D beam problem. In such a study, the solution method presented may be used as an effective tool. Moreover, having extended the plate theories to the cases with nonlocal effect, one may use the associated EBFs in the construction of a boundary layer method for plates. For plate theories based on local elasticity models, the readers may refer to our latest studies (see Shahbazi et al., 2011a,b, 2012; Azhari et al., 2013a,b). The extension of the studies to plates based on nonlocal elasticity models may be performed in a manner analogous to that described in this paper for 2D problems.

As the final remark, the proposed method may be applied to Micro/Nano bars or beams as long as their constitutive equations are written in an integral form similar to the cases studies in this paper.

Appendix A

Consider a system of equations as:

$$\mathbf{KC} = \mathbf{F}, \tag{A-1}$$

where $\mathbf{C}$ is the array of unknown coefficients

$$\mathbf{C} = \{ c_1 \quad c_2 \quad \cdots \quad c_n \}^T, \tag{A-2}$$

$$\mathbf{F} = \{ f_1 \quad f_2 \quad \cdots \quad f_m \}^T, \tag{A-3}$$

and $\mathbf{K}$ is a $m \times n$ matrix. Using a transformation approach (see Boroomand et al., 2010) leads to:

$$c_i = \frac{1}{S_i} \mathbf{k}_i^T \mathbf{R} \mathbf{F}. \tag{A-4}$$

In the above relation, $\mathbf{k}_i$ is a normalized vector which contains the elements of i th column of $\mathbf{K}$ i.e.

$$\mathbf{k}_i = \frac{1}{S_i} \{ k_{1i} \quad k_{2i} \quad \cdots \quad k_{mi} \}^T, \tag{A-5}$$

and $\mathbf{R}$ is defined as

$$\mathbf{R} = \left\{ \sum_{i=1}^{n} (\mathbf{k}_i^T \mathbf{k}_i) \right\}^{-1}. \tag{A-6}$$

The scaling factor S_i may be defined in different ways. One way is the use of the vector length

$$S_i = |\mathbf{k}_i|, \tag{A-7}$$

and another is the use of the maximum element of the vector

$$S_i = \max(|k_{ji}|) \quad j = 1, \ldots, m. \tag{A-8}$$

Appendix B

The roots found for the characteristic equation obtained for the kernel in (56) for various values of L_R/l and ζ_1/ζ_2.

L_R/l	2	3	4	5
$\zeta_1/\zeta_2 = 0$				
αl	±1.0000000000000033	±1.0000000000000033	±1.000000000000003	±1.0000000000000029
	±0.7500099063473225 ±2.6575355619438197**i**	±0.905656896357896 ±1.83920293887541 65**i**	±0.9531906713666723 ±1.4141836016551568**i**	±0.9733926355384206 ±1.1510355857056918**i**
	±0.36802818827062267 ±5.6350627117339 87**i**	±0.7501421880452251 ±3.80994323298947 62**i**	±0.864174819249405 ±2.8921351977918057**i**	±0.9173952940530091 ±2.3365605540363523**i**
	0 ±8.4399469944304 37**i**	±0.6223818041120466 ±5.8513532318924 62**i**	±0.7827002064376666 ±4.4157613380389 29**i**	±0.8608341619245722 ±3.5522737396048103**i**
	0 ±9.0031132757880 65**i**	±0.5213109950646 56**i**	±0.7162734835955787 ±5.9607533929190 74**i**	±0.8120844646951 65 ±4.7848115364940 48**i**
	0 ±11.390660703990642**i**	±0.43710554845346056 ±9.9981965932779 74**i**	±0.6618604868182926 ±7.5158970416634 3**i**	±0.7710379452781077 ±6.0262153462942 83**i**
	0 ±12.285566428487266**i**	±0.36279295174346865 ±12.0827358966046 96**i**	±0.6162078056935647 ±9.0763735518119 01**i**	±0.7361441753973311 ±7.2725553559630 53**i**
	0 ±14.439620721835336**i**	±0.2932090925476748 ±14.1703464796538 5**i**	±0.5769951048056193 ±10.6399261638588 05**i**	±0.7060072339911144 ±8.5218436335631 12**i**
	0 ±15.492163070994035**i**	±0.22309502860561234 ±16.2598191811407 3**i**	±0.5426378591609731 ±12.2053909867540 45**i**	±0.6795754579164436 ±9.7730066808175 5**i**
	0 ±17.524509896288496**i**	±0.14257527749907886 ±18.3504972858630 96**i**	±0.5120368035211996 ±13.7721164647105 78**i**	±0.6560797355993 97 ±11.0254254523944 72**i**
	0 ±18.6731978744342 94**i**	0 ±20.3778734578971 17**i**	±0.4844077140620684 ±15.3397127349700 62**i**	±0.6349539445886521 ±12.2787218817829 82**i**
	0 ±20.6275245428326 56**i**	0 ±22.3767953896171 8**i**	±0.4591747711230398 ±16.9079335717360 5**i**	±0.6157743792185656 ±13.5326536046950 97**i**
	0 ±21.841657252856 05**i**	0 ±24.4207015429019 1**i**	±0.43590369485716474 ±18.4766164239975 77**i**	±0.5982178867983683 ±14.7870587874508 42**i**
	0 ±23.741094004830 85**i**		±0.41425888845784586 ±20.0456499589180 02**i**	±0.5820334387730901 ±16.0418255839619 84**i**
			±0.3939752063884359 ±21.6149555257419 27**i**	±0.5670226965786798 ±17.2968743957278 87**i**
			±0.37483882823391795 ±23.1844760771600 56**i**	±0.5530265254213662 ±18.5521471292176 87**i**
				±0.5399154693834021 ±19.8076004502075 9**i**
				±0.5275829029738841 ±21.0632014115042 45**i**
				±0.5159400217319506 ±22.3189245389506 22**i**

(*continued on next page*)

Appendix B (*continued*)

L_R/l	2	3	4	5
				±0.504912118513924 ±23.57474984091957**i**
$\zeta_1/\zeta_2 = 1/9$ αl	±1.0000000000000036	±1.000000000000003	±1.000000000000003	±1.0000000000000033
	±1.0446603229923976 ±2.5300105606983365**i**	±1.014362769437807 ±1.7593600404414196**i**	±1.0061002197647175 ±1.3600367004436O6**i**	±1.003097853687233 ±1.1123099693939442**i**
	±1.212761565943086 ±5.522152565818341i	±1.0752527344107599 ±3.7216658470612187i	±1.0331418741649436 ±2.8219005547767053i	±1.0168793679868897 ±2.2806556161986116i
	±1.3770980706154181 ±8.633155695122984i	±1.1541794625322213 ±5.776111711410171i	±1.0751528509209405 ±4.3497322157514O4i	±1.0409307425288634 ±3.495134182090785i
	±1.5098161246220128 ±11.766564392255164**i**	±1.2277721593358477 ±7.8566592179839185**i**	±1.1196409775746543 ±5.9030589522280O8**i**	±1.0691853990812599 ±4.732198605408I9**i**
	±1.6176365154666301 ±14.905805478174775**i**	±1.2918456733968098 ±9.94545243483005**i**	±1.161309476762309 ±7.465959808682137**i**	±1.0975479202735638 ±5.9791984633710O8**i**
	±1.7075497291151862 ±18.0469562995158O8**i**	±1.3472955476515207 ±12.0373482934803O7**i**	±1.198947201286801 ±9.0328283364610O5**i**	±1.1243327909645684 ±7.2307302021345I7**i**
	±1.78435083424958 ±21.1888122910271I3**i**	±1.3957053201386997 ±14.130583741849O2**i**	±1.232690841986975 ±10.601525804157O2**i**	±1.1490585363624373 ±8.4844813483370O8**i**
	±1.9104389520991079 ±27.473149488363I8**i**	±1.4384609847870862 ±16.2244575224920O6**i**	±1.263016727751364 ±12.17114528414I6**i**	±1.1717258499097305 ±9.7393996198432I6**i**
		±1.4766467962284173 ±18.31865703225857**i**	±1.2904270435235394 ±13.741263840988653**i**	±1.1925025227323631 ±10.994971158436831**i**
		±1.5110923348115695 ±20.413030335027663**i**	±1.3153644435758547 ±15.311668014384177**i**	±1.2115978477683416 ±12.250928037025625**i**
		±1.542434358594709 ±22.507498557751855**i**	±1.3381981816085888 ±16.882242870615162**i**	±1.2292155301660432 ±13.507122326623971**i**
			±1.3592309896257975 ±18.452923164735786**i**	±1.2455381200180955 ±14.763468245866O4**i**
			±1.378710416112902 ±20.023670214667266**i**	±1.2607238173942392 ±16.019913926435745**i**
			±1.3968396394666511 ±21.594460250455384**i**	±1.2749078700208802 ±17.276426865111I8**i**
			±1.4137865035670625 ±23.165278226926215**i**	±1.2882054129451774 ±18.532986060823I3**i**
				±1.3007145042038513 ±19.789577582558273**i**
				±1.3125189001340465 ±21.046191977144026**i**
				±1.3236904390272104 ±22.302822702943I7**i**

Appendix B (*continued*)

L_R/l	2	3	4	5
$\zeta_1/\zeta_2 = 1/3$				
αl	±1.0000000000000027	±1.0000000000000027	±1.000000000000003	±1.0000000000000024
	±1.3533069035795708 ±2.400074940315497**i**	±1.1625409745983628 ±1.6685803778358281**i**	±1.0904132760478475 ±1.2920432826425619**i**	±1.0559806739026565 ±1.0596096808824 38**i**
	±1.6858807265424596 ±5.457950128946292**i**	±1.346879338927124 ±3.6670793772288497**i**	±1.208141846881463 ±2.7720641897951466**i**	±1.1375605059743488 ±2.2350241496972463**i**
	±1.89250155747435 ±8.5952293913806 38**i**	±1.4725255433736733 ±5.744334034954836**i**	±1.293944353034721 ±4.3193665174391 44**i**	±1.2004473653665195 ±3.4651195677062 63**i**
	±2.0404030498003136 ±11.7401828730406 45**i**	±1.5659481926748986 ±7.835546379148284**i**	±1.359763021986425 ±5.8832277334836 74**i**	±1.2498174772416695 ±4.7123011719374 63**i**
	±2.2488155167112023 ±18.0306676677296 34**i**	±1.639862966815241 ±9.929953167134084**i**	±1.4128595151796817 ±7.4518545667899 03**i**	±1.2903123811554444 ±5.965215061328 02**i**
	±2.3278287996667983 ±21.1751387543016 53**i**	±1.700817543835503 ±12.0251847806171 12**i**	±1.4571840981539919 ±9.022094028983 38**i**	±1.3245233077827034 ±7.2203114750433 52**i**
	±2.3961425183251315 ±24.3191495921638 82**i**	±1.7525901163695283 ±14.1205949599716 69**i**	±1.4951303000054146 ±10.59293808663 5865**i**	±1.3540578156316085 ±8.4763323979 95984**i**
		±1.797540770649007 ±16.2159875657676 87**i**	±1.5282518588883902 ±12.1640168396 8436**i**	±1.3799905859614585 ±9.7327762987 04419**i**
		±1.83723446903521 ±18.31130415334636i	±1.557608495551162 ±13.7351809131 21434i	±1.4030742549845958 ±10.98942321712 7387i
		±1.8727586736329347 ±20.4065323583447i	±1.5839518582682637 ±15.3063663298 69729i	±1.4238541903239992 ±12.2461692943 0918i
		±1.9048980248519725 ±22.5016755653442 25**i**	±1.6078325724630838 ±16.8775450882 00428**i**	±1.4427366523962053 ±13.5029627072 27086**i**
		±1.9612195858838573 ±26.6917410655775 17**i**	±1.6296650849567216 ±18.4487052777 3847**i**	±1.4600314568077468 ±14.7597765700 35362**i**
			±1.6497686132827838 ±20.0198424668729 66**i**	±1.4759797055314243 ±16.0165966027 21176**i**
			±1.6683939382600073 ±21.5909557556 81527i	±1.4907723738050933 ±17.2734151707 70562i
			±1.6857414801372705 ±23.1620458901 57856i	±1.504563100802113 ±18.5302282571 51936i
				±1.5174771986278042 ±19.7870338595 38628**i**
				±1.5296181307657593 ±21.0438311129 39202**i**
				±1.5410722584367356 ±22.3006197962 4988**i**
				±1.5519123769445544 ±23.5574000488 40965**i**
$\zeta_1/\zeta_2 = 1$				

(*continued on next page*)

Appendix B (*continued*)

L_R/l	2	3	4	5
αl	±1.000000000000003	±1.0000000000000027	±1.0000000000000024	±1.0000000000000027
	±1.8007686698647412 ±2.2374174209170485**i**	±1.4155910166431467 ±1.5473603640674178**i**	±1.2540693013946842 ±1.19480287860014 61**i**	±1.1702296356016455 ±0.9789923392210208**i**
	±2.212188436059876 ±5.396964596979994**i**	±1.6791145381027652 ±3.617487478055173**i**	±1.443033851253834 ±2.7267024212266255**i**	±1.3144870861488571 ±2.19191456694033**i**
	±2.4323020390114456 ±8.559683704254432**i**	±1.8230250086782198 ±5.7169341508071865**i**	±1.5487069586666031 ±4.294782204766678**i**	±1.3973782811770035 ±3.441419083077462**i**
	±2.5846630001651585 ±11.7151755970230 94**i**	±1.9232814135045175 ±7.817083025958386**i**	±1.622692871132358 ±5.8672892041319535**i**	±1.4555924280889623 ±4.697279947799958**i**
	±2.701406862103256 ±14.866347208604237**i**	±2.0004241550988078 ±9.916089154996351**i**	±1.6798634876744227 ±7.440264704831341**i**	±1.5007215184052134 ±5.954593447090945**i**
	±2.7960681117218775 ±18.014922551968642**i**	±2.0631382845730717 ±12.014085363521632**i**	±1.7264843828076029 ±9.013032909058431**i**	±1.5376298034449067 ±7.212208876583988**i**
	±2.875678303777353 ±21.161837823762 19**i**	±2.115968521649268 ±14.111333839795202**i**	±1.7658416916806097 ±10.585507134709404**i**	±1.5688579073778677 ±8.469817685924582**i**
	±2.944367578376656 ±24.307630287909 19**i**	±2.161601704783878 ±16.208036416643 63**i**	±1.7998881413274803 ±12.157717566028342**i**	±1.5959174737630828 ±9.727338943419351**i**
		±2.201760194908874 ±18.304334147144 83**i**	±1.8298819550014538 ±13.729711325967 59**i**	±1.6197858942532106 ±10.984759278071516**i**
		±2.2376145382499764 ±20.400325125192424**i**	±1.8566820003366091 ±15.301530690150456**i**	±1.641132895986572 ±12.2420854818029 19**i**
		±2.2699964648261344 ±22.496078697408407**i**	±1.880900719152259 ±16.873209638409445**i**	±1.6604377300199924 ±13.499329382100 74**i**
			±1.9029901366829232 ±18.444774679973 61**i**	±1.6780551906852348 ±14.756502930566322**i**
			±1.9232933381963446 ±20.016246402781217**i**	±1.6942552525567347 ±16.013616735563673**i**
				±1.7092480790698423 ±17.270679782148726**i**
				±1.7232004473461628 ±18.527699545104998**i**
				±1.7362469005294412 ±19.784682208701252**i**
				±1.748497536482407 ±21.041632891735585**i**
$\zeta_1/\zeta_2 = 3$				
αl	±1.0000000000000033	±1.0000000000000036	±1.0000000000000029	±1.0000000000000024
	±2.3510160002935123 ±2.085772283583867**i**	±1.7583775018336396 ±1.4303542669388192**i**	±1.4954004172962836 ±1.0974124030058923**i**	±1.3521147771990374 ±0.8949204868076359**i**
	±2.762215776035338 ±5.342086034380193**i**	±2.039051706385531 ±3.576185637489402**i**	±1.7077952156711245 ±2.6912805262243524**i**	±1.5222283034059836 ±2.1595488990947636**i**

Appendix B (*continued*)

L_R/l	2	3	4	5
	±2.9822114428605837 ±8.52641219504325**i**	±2.1862917957455297 ±5.693016087954328**i**	±1.8183115378742678 ±4.2749876664628 91**i**	±1.6106419394227947 ±3.4236819934679414**i**
	±3.134475863396614 ±11.6912420769163 57**i**	±2.287859517633266 ±7.80032078778802**i**	±1.894359442144438 ±5.8538109251868 68**i**	±1.6713369733394665 ±4.6855124896604 23**i**
	±3.2511336429941116 ±14.8476285247239 8**i**	±2.36562656045945 ±9.9031735763840 13**i**	±1.952576891519078 ±7.4300758701912 22**i**	±1.7177877018934422 ±5.945880196325 52**i**
	±3.345725135188268 ±17.9995394912320 63**i**	±2.428677304135696 ±12.0035677618199 71**i**	±1.9997906302941237 ±9.0048394904398 44**i**	±1.7554703524550366 ±7.2053066951450 93**i**
	±3.42528029007195 ±21.1487751317516 13**i**	±2.4817061302673262 ±14.1024555472359 3**i**	±2.039511826619367 ±10.5786495512518 04**i**	±1.7871854578374438 ±8.4641030302571 21**i**
	±3.4939261360209937 ±24.2962765084498 1**i**	±2.527464669264908 ±16.2003508837371 05**i**	±2.073795841208703 ±12.1518167581892 8**i**	±1.8145688050180195 ±9.7224602856247 04**i**
	±3.608165721814353 ±30.5880382147325 6**i**	±2.5677065446158553 ±18.2975562109960 03**i**	±2.103952452665295 ±13.7245299462109 73**i**	±1.8386622943491833 ±10.9805005327860 44**i**
	±3.6568029026886832 ±33.7328530145218 4**i**	±2.6036187148741385 ±20.3942614471751 04**i**	±2.1308684876385504 ±15.2969103534998 77**i**	±1.8601715287911642 ±12.2383047980960 9**i**
		±2.636042125421227 ±22.4905920597026 35**i**	±2.1551725212542383 ±16.8690393626798 78**i**	±1.879596864809087 ±13.4959285775302 51**i**
		±2.665594370351241 ±24.5866343855074 23**i**	±2.177326376401607 ±18.4409736466591 8**i**	±1.8973061116516807 ±14.7534118507268 49**i**
			±2.197679347994437 ±20.0127539030108 96**i**	±1.9135775962637183 ±16.0107827680320 65**i**
			±2.2165020258180057 ±21.5844101285934 6**i**	±1.9286270281835463 ±17.2680628695098 55**i**
			±2.234008291129199 ±23.1559649324285 78**i**	±1.9426249772146784 ±18.5252683835873 1**i**
				±1.9557086474031493 ±19.7824118617419 7**i**
				±1.9679900458957353 ±21.0395031658679 4**i**
				±1.9905013630978372 ±23.5535591663056**i**

Appendix C

The roots found for the characteristic equation (59) for various values of L_R/l and $\zeta_1 = 0$.

L_R/l	2	3	4	5
$\zeta_1/\zeta_2 = 0$ αl	±1.2915296675598191 ±3.9816882188872 11**i**	±3.2903797434298014 ±3.9829336852788852**i**	±5.290379743775968 ±3.9829336856677524**i**	±7.29037974377595 ±3.9829336856677 76**i**
	0	±1.6459090973813402	±3.645910187820739	±5.6459101878207365

(*continued on next page*)

(**Appendix C** *continued*)

L_R/l	2	3	4	5
	±5.233282600551831**i**	±5.382308898639397**i**	±5.382298048502862**i**	±5.3822980485028875**i**
	0	±0.4375843965304682	±2.4312247738025885	±4.431224773539111
	±6.568961294866879**i**	±6.485734350807826**i**	±6.470661737220807**i**	±6.47066173670564**i**
	0	0	±1.425180267587381	±3.425178421220269
	±8.093988148263742**i**	±7.574382259341356**i**	±7.394619184806986**i**	±7.394619404936927**i**
	0	0	±0.5499477701218822	±2.5481025611077786
	±9.628612943372627**i**	±8.586502575424388**i**	±8.211269579334752**i**	±8.2122145693662 44**i**
	0	0	0	±1.7607295466014463
	±11.172250197424377**i**	±9.615553881943761**i**	±8.888813903666636**i**	±8.9536313883713 24**i**
	0	0	0	±1.0403383393536816
	±12.72205959026841**i**	±10.646985490939587**i**	±9.599222628107569**i**	±9.6369778490360 77**i**
	0	0	0	±0.37558133419576467
	±14.276218192672276**i**	±11.680598529418344**i**	±10.377271042080327**i**	±10.2746116907863 15**i**
	0	0	0	0
	±15.833531041275007**i**	±12.71601624239391**i**	±11.153680398733716**i**	±10.8614457263673 18**i**
	0	0	0	0
	±17.39319369021036**i**	±13.752932068327812**i**	±11.930921583108 26**i**	±11.4538975915413 42**i**
	0	0	0	0
	±18.95464904890363**i**	±14.791097137255392**i**	±12.708861433119134**i**	±12.0780010272846 51**i**
	0	0	0	0
	±20.517500891288 30**i**	±15.830309912871558**i**	±13.487428584573049**i**	±12.7012630572828 26**i**
	0	0	0	0
	±22.081460516496 12**i**	±16.870406937349 29**i**	±14.266557795943392**i**	±13.3248475524261 7**i**
	0	0	0	0
	±23.646312989973737**i**	±17.911255118857 98**i**	±15.046190648891086**i**	±13.9487046052391 68**i**
		0	0	0
		±18.952745521488282**i**	±15.826275123311564**i**	±14.5728165212400 07**i**
		0	0	0
		±19.994788449975584**i**	±16.606765063465144**i**	±15.1971659318853 2**i**
		0	0	0
		±21.037309588815464**i**	±17.387619600993876**i**	±15.8217365216265 67**i**
		0	0	0
		±22.080246975805508**i**	±18.168802581723 47**i**	±16.4465130270062 55**i**
		0	0	0
		±23.123548626589727**i**	±18.950282023015774**i**	±17.0714812225147**i**
			0	0
			±19.732029615313 74**i**	±17.6966278884845 2**i**
			0	0
			±20.514020273263 09**i**	±18.3219407671124 9**i**
			0	0
			±21.296231736830617**i**	±18.9474085111232 07**i**

(**Appendix C** *continued*)

L_R/l	2	3	4	5
			0 ±22.078644220032903**i**	0 ±19.573020628454568**i**
			0 ±24.42692085253052**i**	0 ±20.198767425439836**i**
				0 ±20.82463995025338**i**
				0 ±21.450629937843345**i**
				0 ±24.582094209876782**i**

In the above relations |.| denotes the Hermitian length. This latter form has been used in the numerical examples of this paper.

In problems with Neumann boundary conditions the **D** matrix in (96) plays the role of a multiplier compared with the values in (98). This is mainly because in practice the value of Young's modulus, E, is large and this effect may introduce some numerical errors in the computations. The effect may be removed by multiplying the Dirichlet boundary conditions by E i.e.

$$E\sum_i c_i \mathbf{h}^i e^{\alpha_i x_B+\beta_i y_B} = E\left(\mathbf{u}_B - \sum_{r,s}\mathbf{h}_{rs} e^{\alpha_r x_B+\beta_s y_B}\right), \tag{A-9}$$

or alternatively by dividing (95) and (96) by E.

References

Abdollahi, R., Boroomand, B., 2013. Benchmarks in nonlocal elasticity defined by Eringen's integral model. Int. J. Solids Struct. 50, 2758–2771.

Altan, S.B., 1989. Uniqueness of initial-boundary value problems in nonlocal elasticity. Int. J. Solids Struct. 25, 1271–1278.

Azhari, F., Boroomand, B., Shahbazi, M., 2013a. Exponential basis functions in the solution of laminated plates using a higher-order Zig–Zag theory. Compos. Struct. 105, 398–407.

Azhari, F., Boroomand, B., Shahbazi, M., 2013b. Explicit relations for the solution of laminated plates modeled by a higher shear deformation theory: derivation of exponential basis functions. Int. J. Mech. Sci. 77, 301–313.

Bažant, Z.P., Jirásek, M., 2002. Nonlocal integral formulations of plasticity and damage: survey of progress. ASCE J. Eng. Mech. 128, 1119–1149.

Benvenuti, E., Tralli, A., 2006. The fast Gauss transform for non-local integral FE models. Commun. Numer. Methods Eng. 22, 505–533.

Benvenuti, E., Simone, A., 2013. One-dimensional nonlocal and gradient elasticity: closed-formsolution and size effect. Mech. Res. Commun. 48, 46–51.

Borino, G., Failla, B., Parrinello, F., 2003. A symmetric nonlocal damage theory. Int. J. Solids Struct. 40, 3621–3645.

Boroomand, B., Noormohammadi, N., 2013. Weakly equilibrated basis functions for elasticity problems. Eng. Anal. Bound. Elem. 37, 1712–1727.

Boroomand, B., Soghrati, S., Movahedian, B., 2010. Exponential basis functions in solution of static and time harmonic elastic problems in a meshless style. Int. J. Numer. Methods Eng. 81, 971–1018.

Boyd, J.P., 2000. Chebyshev and Fourier Spectral Methods. Dover Publications.

Brebbia, C.A., Dominguez, J., 1998. Boundary Elements an Introductory Course, second ed. WIT Press, Computational Mechanics Publications, Southampton.

Challamel, N., 2013. Variational formulation of gradient or/and nonlocal higher-order shear elasticity beams. Compos. Struct. 105, 351–368.

Challamel, N., Casandjian, C., Lanos, C., 2009a. Some closed-form solutions to simple beam problems using nonlocal (gradient) damage theory. Int. J. Damage Mech. 18, 569–598.

Challamel, N., Rakotomanana, L., Marrec, L.L., 2009b. A dispersive wave equation using nonlocal elasticity. C. R. Mecan. 337, 591–595.

Challamel, N., Wang, C.M., 2008. The small length scale effect for a non-local cantilever beam: a paradox solved. Nanotechnology 19, 345703.

Chen, J.T., Lee, Y.T., Yu, S.R., Shieh, S.C., 2009. Equivalence between the Trefftz method and the method of fundamental solution for the annular Green's function using the addition theorem and image concept. Eng. Anal. Bound. Elem. 33, 678–688.

Edelen, D.G.B., Green, A.E., Laws, N., 1971. Nonlocal continuum mechanics. Arch. Rat. Mech. Anal. 43, 36–44.

Edelen, D.G.B., Laws, N., 1971. On the thermodynamics of systems with nonlocality. Arch. Rat. Mech. Anal. 43, 24–35.

Eringen, A.C., 1987. Theory of nonlocal elasticity and some applications. Res. Mech. 21, 313–342.

Eringen, A.C., 2002. Nonlocal Continuum Field Theories. Springer.

Eringen, A.C., Edelen, D.G.B., 1972. On nonlocal elasticity. Int. J. Eng. Sci. 10, 233–248.

Eringen, A.C., Kim, B.S., 1974. Stress concentration at the tip of crack. Mech. Res. Commun. 1, 233–237.

Eringen, A.C., Speziale, C.G., Kim, B.S., 1977. Crack-tip problem in non-local elasticity. J. Mech. Phys. Solids 25, 339–355.

Fairweather, G., Karageorghis, A., 1998. The method of fundamental solutions for elliptic boundary value problems. Adv. Comput. Math. 9, 69–95.

Hashemi, S.H., Boroomand, B., Movahedian, B., 2013. Exponential basis functions in space and time: a meshless method for 2D time dependent problems. J. Comput. Phys. 241, 526–545.

Jirásek, M., Rolshoven, S., 2003. Comparison of integral-type nonlocal plasticity models for strain-softening materials. Int. J. Eng. Sci. 41, 1553–1602.

Kita, E., 1995. Trefftz method: an overview. Adv. Eng. Softw. 24, 3–12.

Kröner, E., 1967. Elasticity theory of materials with long range cohesive forces. Int. J. Solids Struct. 3, 731–742.

Krumhansl, J.A., 1968. Some considerations on the relations between solid state physics and generalized continuum mechanics. In: Kroner, E. (Ed.), Mechanics of Generalized Continua. Springer, Berlin, pp. 298–331.

Kunin, I.A., 1984. On foundations of the theory of elastic media with microstructure. Int. J. Eng. Sci. 22, 969–978.

Kupradze, V.D., Aleksidze, M.A., 1964. The method of functional equations for the approximate solution of certain boundary value problems. USSR Comput. Math. Math. Phys. 4, 82–126.

Lazar, M., Maugin, G., Aifantis, E.C., 2006. On a theory of nonlocal elasticity of bi-Helmholtz type and some applications. Int. J. Solids Struct. 43, 1404–1421.

Movahedian, B., Boroomand, B., Soghrati, S., 2013. A Trefftz method in space and time using exponential basis functions: application to direct and inverse heat conduction problems. Eng. Anal. Bound. Elem. 37, 868–883.

Movahedian, B., Boroomand, B., 2014. The solution of direct and inverse transient heat conduction problems with layered materials using exponential basis functions. Int. J. Therm. Sci. 77, 186–198.

Pisano, A.A., Fuschi, P., 2003. Closed form solution for a nonlocal elastic bar in tension. Int. J. Solids Struct. 40, 13–23.

Pisano, A.A., Sofi, A., Fuschi, P., 2009. Nonlocal integral elasticity: 2D finite element based solutions. Int. J. Solids Struct. 46, 3836–3849.

Polizzotto, C., 2001. Nonlocal elasticity and related variational principles. Int. J. Solids Struct. 38, 7359–7380.

Schwartz, M., Niane, N.T., Kouitat Njiwa, R., 2012. A simple solution method to 3D integral nonlocal elasticity: isotropic-BEM coupled with strong form local radial point interpolation. Eng. Anal. Bound. Elem. 36, 606–612.

Shahbazi, M., Boroomand, B., Soghrati, S., 2011a. A mesh-free method using exponential basis functions for laminates modeled by CLPT, FSDT and TSDT – Part I: Formulation. Compos. Struct. 93, 3112–3119.

Shahbazi, M., Boroomand, B., Soghrati, S., 2011b. A mesh-free method using exponential basis functions for laminates modeled by CLPT, FSDT and TSDT – Part II: Implementation and results. Compos. Struct. 94, 84–91.

Shahbazi, M., Boroomand, B., Soghrati, S., 2012. On using exponential basis functions for laminates modeled by CLPT, FSDT and TSDT: further tests and results. Compos. Struct. 94, 2263–2268.

Shamsaei, B., Boroomand, B., 2011. Exponential basis functions in solution of laminated structures. Compos. Struct. 93, 2010–2019.

Zandi, S.M., Boroomand, B., Soghrati, S., 2012a. Exponential basis functions in solution of incompressible fluid problems with moving free surfaces. J. Comput. Phys. 231, 505–527.
Zandi, S.M., Boroomand, B., Soghrati, S., 2012b. Exponential basis functions in solution of problems with fully incompressible materials: a mesh-free method. J. Comput. Phys. 231, 7255–7273.
Zielinski, A.P., Herrera, I., 1987. Trefftz method: fitting boundary conditions. Int. J. Numer. Methods Eng. 24, 871–891.
Zingales, M., Di Paola, M., Inzerillo, G., 2011. The finite element method for the mechanically based model of non-local continuum 2011. Int. J. Numer. Methods Engng. 86, 1558–1576.